Geomorphology 317 (2018) 23–44

Contents lists available at ScienceDirect

Geomorphology

journal homepage: www.elsevier.com/locate/geomorph

Invited research article

Using textural analysis for regional landform and landscape mapping, Eastern Guiana Shield

Pierre Bugnicourt [a,*], Stéphane Guitet [a], Valdenira F. Santos [b], Lilian Blanc [c], Eleneide D. Sotta [d], Nicolas Barbier [a], Pierre Couteron [a]

[a] AMAP, IRD, CIRAD, CNRS, INRA, Univ Montpellier, Montpellier, France
[b] Instituto de Pesquisas Científicas e Tecnológicas do Estado do Amapá (IEPA), Macapá, Amapá, Brazil
[c] FS, Cirad, Baillarguet, France
[d] Empresa Brasileira de Pesquisa Agropecuaria (Embrapa), Macapá, Amapá, Brazil

ARTICLE INFO

Article history:
Received 25 September 2017
Received in revised form 21 March 2018
Accepted 21 March 2018
Available online 29 March 2018

Keywords:
SRTM/DEM
Land surface texture
Semi-automated mapping
FOTO method
Terrain grain
Relief criteria

ABSTRACT

Availability of digital elevation models (DEM) of increased spatial resolution has triggered interest in texture-based methods for automated geomorphometry. This prospect is all the more appealing concerning tropical countries for which mapping of geomorphic entities has remained limited despite its relevance for natural resource assessment and land planning. In this paper we applied to the Shuttle Radar Topography Mission (SRTM) DEM a multiscale texture analysis based on Fourier 2D periodogram (FOTO method) to reach a spatially coherent mapping that would agree with current knowledge over the conterminous territories of French Guiana and Amapa (Brazil). Through a principal component analysis, FOTO-extracted textural features were found complementary and combined with six common physiographic criteria (convexity, wetness index, dissection, elevation, and percent of steep and low slopes) calculated from the DEM. This provided a primary semiautomated mapping of 16 classes of landform types. To increase legibility, we aggregated into eight landscape unit classes that were the most similar in terms of texture and relief criteria while being frequently contiguous. The resulting map was compared with existing maps that were, however, more local or of lesser resolution and informative content over the region of interest. Multiscale Fourier spectra proved useful to depict land surface texture and, in synergy with relief variables, allowed identifying a large variety of landforms for broad-scale geomorphic mapping in the humid tropics.

1. Introduction

General geomorphometry is the measurement and analysis of landform characteristics that are applicable to any continuous rough surface (Mark, 1975). The worldwide availability of DEM now calls for designing methods to efficiently apply geomorphometry principles in territories for which geormorphic mapping is underdeveloped and lacking. This lack of geomorphological studies and maps is particularly apparent within the humid tropical regions that are much diversified (Thomas, 2006; Migon, 2009). This geomorphological diversity (Panizza, 2009) is explained by the various processes of morphogenesis (climate change, tectonic history) impacting the region differently depending on the lithology (Walsh and Blake, 2009). These processes lead to a diversity of landforms as natural objects partitioning the earth surface and defining boundary conditions for processes operative in the fields of geomorphology, hydrology, ecology, pedology and others (MacMillan and Shary, 2008; Dragut and Eisank, 2012). In Amazonia, geomorphological diversity proved to be an important explanatory factor for differences in forest ecosystem functioning and spatial biodiversity patterns (Slaymaker et al., 2009) observed at local (Sabatier, 2006; Guitet et al., 2015b) and regional scales (Hammond, 2005). At the local scale (landforms <1 km^2), soil cover varies along the *catena* depending on the position on the landform and exerts an abiotic filter on the local assemblages of vegetal species (Sabatier et al., 1997). At the intermediate scale (i.e., 1–1000 km^2), differences in landform assemblages owing to erosional, hydrological, and weathering histories inform on forest dynamics and influence forest structure (Paget, 1999; Bispo et al., 2016). At broad scales (>1000 km^2), the diversity of geomorphological landscapes is relevant to understand the establishment of present biogeographic zones, explain floristic composition patterns, and help understand spatial variation in carbon stocks (Hammond, 2005; Figueiredo et al., 2013; Guitet et al., 2015a). As a consequence, the development of large-scale geomorphological analyses (at regional or continental scale) is necessary to better understand the past, current, and future functioning of tropical forest ecosystems in the context of global changes (Slaymaker et al., 2009) and have better tools to manage

* Corresponding author at: Université de Montpellier, UMR Botany and Modeling of the Architecture of Plants and Vegetations (AMAP), F-34000 Montpellier, France.
E-mail address: pierre.bugnicourt@gmail.com (P. Bugnicourt).

https://doi.org/10.1016/j.geomorph.2018.03.017
0169-555X/

lands, resources, and ecosystem services. Unfortunately, the geomorphological maps that are available at large scales in many forested tropical territories, of sparse population and limited accessibility, are generally old and expert-based products of low mapping resolution. Products based on expert knowledge often follow aims and methods specific to each country or region and are difficult to compare or harmonize over large, transborder areas. This situation makes geomorphology underused in biodiversity and conservation studies as well as in natural resource assessment and land planning.

Thanks to airborne or space observation, the increased availability of DEMs covering a large range of scales opens avenues to address semi-automated geomorphological mapping at broad scale. The strength of the semi-automatic methods is to generate maps that are consistent over space and comparable across different regions. The availability of DEMs has triggered burgeoning interest for algorithms aimed at extracting geomorphometric signatures from land surface data. A large share of these studies have dealt with small to intermediate scales of 100–1000 km^2 using DEMs of high spatial resolution (often cells of 1 m or less in the field) to accurately locate and map particular geomorphic entities such as landslides and valleys (Perron et al., 2008; Booth et al., 2009; Trevisani et al., 2012).

Studies targeting broader scales and a variety of geomorphic entities have been comparatively rare in spite of the provision of the Shuttle Radar Topography Mission (SRTM) data by the National Aeronautics and Space Administration (Farr et al., 2007; NASA, 2013), with spatial resolution (cell size) of ca. 30 m (1 arcsec) (released by NASA, 2013). While SRTM DEMs provide avenues for landform classifications at regional and global scales (Dragut and Eisank, 2012), few studies have aimed at worldwide mapping following the pioneering work of Iwahashi and Pike (2007). Moreover, the design of these products targeting a global scale is irrelevant for regional uses, especially in the Amazonian region that appears, wrongly, as uniform in Dragut and Eisank (2012) or that expresses noisy patterns in Iwahashi and Pike (2007). However, the vision underlying these recent developments, i.e., designing meaningful geomorphic features for computation from SRTM elevation data, is far reaching and shows the potential of these data for automated extraction of geomorphic signatures over territories devoid of adequate landform or landscape mapping. More specifically, Dragut and Eisank (2012) emphasized that using SRTM elevation as a single input variable can lead to reasonable results (through object-oriented classification). Iwahashi and Pike (2007) introduced elevation-derived surface texture among three input geometric criteria (Pike, 1988) of an automated algorithm. But several aspects of the texture concept (Haralick et al., 1973) have not been considered by these last authors who limited themselves to the frequency analysis of pits and peaks for processing SRTM elevation data. Several well-established approaches to image texturing based on geostatistical functions (Balaguer et al., 2010; Trevisani et al., 2012), grey level co-occurrence matrix (i.e., GLCM; Haralick et al., 1973; Hua et al., 2006), wavelets (e.g., Ollier et al., 2003; Jordan and Schott, 2005), or Fourier 2D Periodogram or power spectrum (Couteron et al., 2006; Perron et al., 2008; Booth et al., 2009) can help extract more information than in Iwahashi and Pike (2007). Although Fourier analysis has long been considered (Evans, 1972; Mark, 1975) and used in geomorphology (e.g., Hanley, 1977; Harrison and Lo, 1996), its usage remained rare and confined to the most straightforward application detecting and quantifying quasi-periodic patterns such as knolls, ridges, or valleys (Hanley, 1977; Mugglestone and Renshaw, 1998; Perron et al., 2008). However, landscape ecology recognizes that Fourier spectra are generally informative on very diverse types of spatial patterns ranging from quasi-periodic to scaleless (i.e., fractal-like) (Keitt, 2000; Couteron et al., 2006). This supports the opinion of Perron et al. (2008) that Fourier spectral analysis is a robust means of analyzing topographic attributes and provides measurements for structures that have remained difficult to be objectively quantified, albeit often being visually apparent.

In this paper, we use Fourier spectra provided by the two-dimensional Discrete Fourier Transform (DFT) to address the mapping of landform and landscape-based spatial entities (MacMillan et al., 2003) calculated from SRTM elevation in tropical South America. We show that the multivariate comparison of many such spectra (Fourier-based Textural Ordination, FOTO method; Couteron, 2002; Couteron et al., 2006) can provide robust, multiscale texture indices of topography (or terrain grain). Furthermore, we will show that these indices are relevant for characterizing simultaneously landform shapes, repetitions, and spatial connectivity (here referred to as "landform-types"). We combine such texture indices with six common physiographic criteria (or geometric signatures sensu Pike, 1988) to reach landform-type mapping, which will be further simplified into a map of landscape units.

We applied our approach to a large northeastern part of the Guiana shield (220,000 km^2), made of French Guiana and the Brazilian state of Amapa, which is largely covered by forests. As for a large share of the humid tropics, consistent mapped information on relief, soils, and vegetation are not available for natural resource assessment and land planning that would concern both territories. Previous studies in French Guiana have proven that the mapping of landforms and landscapes is relevant for understanding spatial patterns of biodiversity and forest resources (Slaymaker et al., 2009; Sabatier, 2006; Guitet et al., 2015b). For this, a detailed geomorphological object-based map of landscapes is already available over French Guiana ca. 83,000 km^2 (Guitet et al., 2013). This map was established from SRTM digital elevation data using an object-based identification of individual landforms coupled with a multivariate analysis and expert delineation of broader entities, called landscape classes. Extending this quite heavy mapping process to larger parts of the Guiana shield in neighboring countries is limited by insufficient availability of experts and trained operators as often in tropical countries. Our aim is to demonstrate here that texture analysis makes it possible to semi-automatically map landforms from SRTM data in a way reproducible over very large areas as to help in assessing natural resources and biodiversity in the humid forested tropical landscapes.

2. Materials and methods

2.1. Study area

Our study area included French Guiana (83,000 km^2) and the adjacent federal state of Amapa (142,000 km^2, Brazil) in northeastern South America (Fig. 1). Amapa is delimited in the southeast by the Amazon River and to the northeast by the Atlantic Ocean. The Jari River in the southwest and west marks the frontiers with the federal Brazilian state of Para. French Guiana is located between the Oiapoque River in the east (border with Amapa) and the Maroni River in the west (border with Suriname). Southward it borders with Amapa through the 'Tumuc – Humac' mountains (Fig. 1). The two territories are located between 6°N and 1°5′S and between 55°W to 49°5′W. Equatorial climate is prevalent over both territories. Combined with proximity to the Atlantic Ocean, it induces high annual rainfall (usually >2000 mm) and high humidity because of high and quite stable temperatures throughout the year (mean > 20 °C every month).

Amapa and French Guiana extend over the low eastern part of the Guiana shield (Fig. 1) (Paget, 1999; Delor et al., 2003) where the ancient Precambrian crust is >2 Gy old and close to 3 Gy old southeast of Amapa (Santos et al., 2000). The Guiana shield is highly eroded and low elevated (maximum height about 850 m asl in our area) and has experienced volcanic, plutonic, and metamorphic episodes during "paleoproterozoic" (Delor et al., 2003). It is organized in three main belts, parallel to the eastern coastal plain, separated by three synclinorium. The first belt, adjacent to the coastal plain, is composed of low granitic plateaus (about 100 m asl) of lower Proterozoic (IBGE, 2004). It is delimited by a northern synclinorium in French Guiana (Paget, 1999), with volcano-sedimentary origin and covered by lateritic crust up to 500 m elevation (Choubert, 1957). Next to the first belt, a

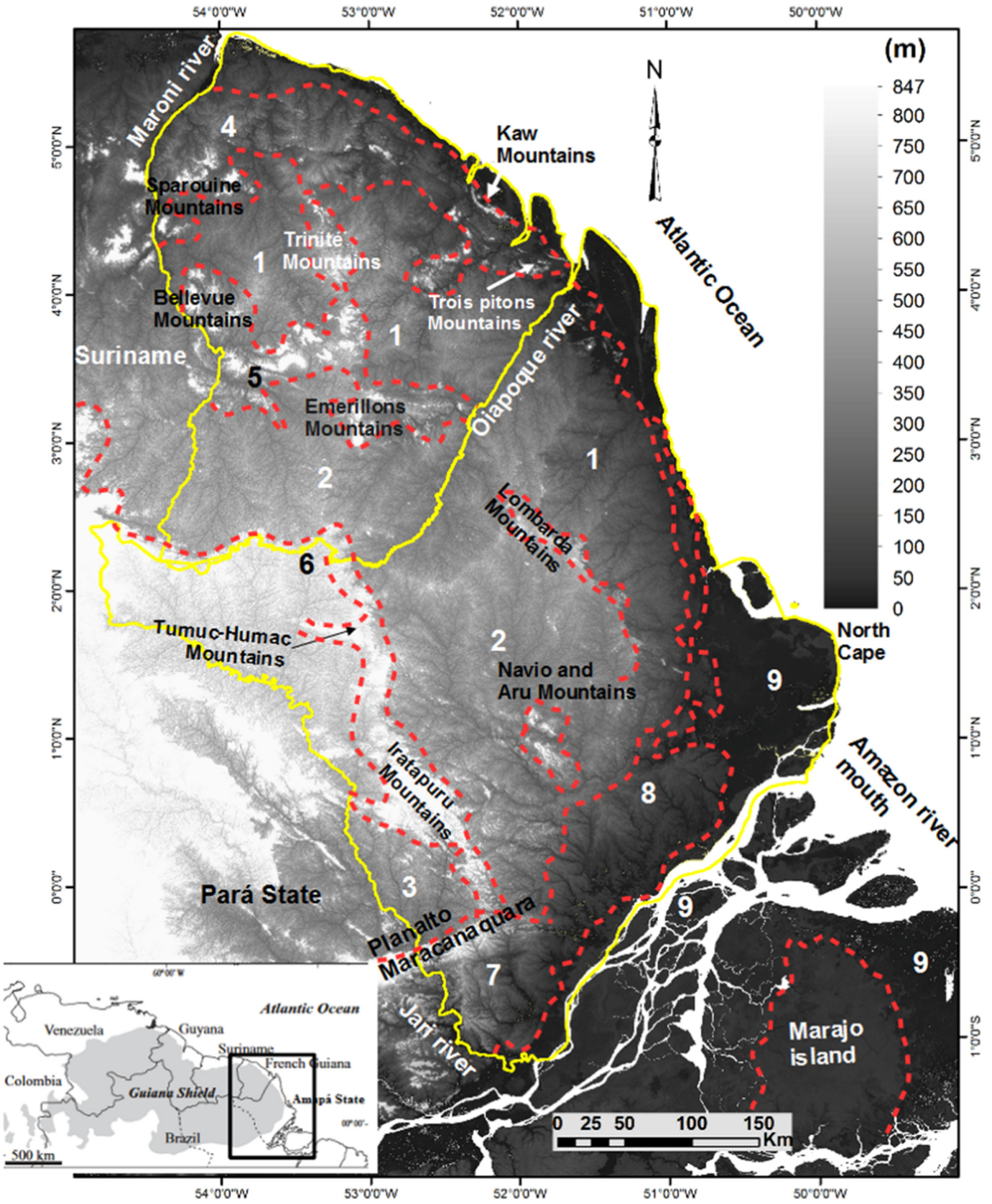

Fig. 1. Simplified morphostructural sketch map of the Eastern Guiana shield. 1) Guiana shield: granitic plateau I; 2) Guiana shield: granitic plateau II; 3) Guiana shield: septentrional amazonian depression; 4) Guiana shield: northern synclinorium; 5) Guiana shield: southern synclinorium and central mountain range; 6) Guiana shield: Tumuc-Humac synclinorium; 7) Phanerozoic sediments: Amazon sedimentary basin; 8) Phanerozoic sediments: Amapá coastal tableland; 9) Phanerozoic sediments: Quaternary coastal plain. From: Magnani, 1952; Boaventura and Narita, 1974; Paget, 1999; Santos et al., 2000; Delor et al., 2003; IBGE, 2004.

suite of mountain ranges features the southern synclinorium (with some areas about 500 m asl) in French Guiana (Paget, 1999) that is linked to Serra Lombarda in the center of Amapa (IBGE, 2004). These ranges separate the first belt from the more inland second belt, which is a large granitic plateau in the central area of Amapa State and the southern part of French Guiana (about 200 m asl) (Paget, 1999; IBGE, 2004). This plateau becomes a low-relief plain on the French Guiana side (Guitet et al., 2013). The large area of "Amapa's hills" (IBGE, 2004) occurs between the first and second belts. In these belts, the networks of rivers connect the Guiana shield to the ocean through grand rivers such as Oiapoque and Maroni. The third belt, exclusively in Amapa, is the Tumuc-Humac synclinorium with the highest elevation observed in the Amapa territory (closer than 650 asl) and is bordered by the Tumuc-Humac Mountains (south of French Guiana) and Serra Iratapuru Mountains (IBGE, 2004).

Tabular and residual reliefs occur in southern Amapa on Paleozoic and Cenozoic rocks of the Amazon basin (Gibbs and Barron, 1993; IBGE, 2004). Here, the tabular relief of Maracanaquara plateau delimit the southern border of Guiana shield (Fig. 1). In the state of Amapa, unconsolidated Pleistocene sediments constitute the Quaternary coastal plain that is characterized in the North Cape by several lakes connecting the main rivers of the mouth of the Amazon. This coast is highly floodable, especially along the Amazon River and its mouth, mainly owing to the slight elevation (Magnani, 1952; Boaventura and Narita, 1974; Jardim et al., 2015).

2.2. Data

Analyses were performed from the SRTM data acquired by NASA in February 2000 (see Farr et al., 2007 for technical details) at the increased resolution of 1 arcsec (published for open access by NASA in 2013). Such data approximates the elevation at the top of vegetation. The vertical accuracy of SRTM data has been assessed as being about 10 m for the 3 arcsec version (Bourgine and Baghdadi, 2005). We used data at 1 arcsec as digital elevation model (DEM) as variations of canopy height are small over the dense humid tropical forest. Indeed, canopy height variation among five broad forest types in French Guiana were barely detectable from the 3 arcsec SRTM (Fayad et al., 2014). The elevation data may, however, include spatial variation in vegetation height in coastal areas where landscapes include forest and nonforest mosaics. For training purposes, we used a geomorphological map previously produced across French Guiana (Guitet et al., 2013) from the same DEM but using a complex object-based approach that could refer to field transects for validation. We also scanned geomorphological maps of Amapa (scale 1:750,000) produced by Instituto Brasileiro de Geografia e Estatística (IBGE) in 2004 and the recent version for 'Amazônia Legal' delivered in electronic vectors in 2015 for comparisons purposes.

2.3. Textural analysis

Using textural analysis, we wanted to characterize *geometric signatures*, i.e., 'a set of measures that describes topographic form well enough to distinguish geomorphologically disparate landscapes' (Pike, 1988). Signatures allowed us to identify what we call here landform types that are assemblages of repeating patterns of landform elements with characteristic patterns and scales of repetition (MacMillan et al., 2000).

For textural analysis of the SRTM, we used Fourier-based textural ordination (FOTO; Couteron, 2002; Couteron et al., 2006), which is here applied for the first time in the field of geomorphometry. As illustrated in Fig. 2, FOTO subdivides the SRTM image in square windows (A) of chosen dimensions and analyzes spatial variations of the SRTM grey levels (i.e., elevation values) for each window. These variations characterize landforms, their shapes and their repetitiveness in the analysis window. They are decomposed by the two-dimensional Discrete Fourier Transform (2D DFT, Fig. 2B) in a space of sine/cosine waveforms having harmonic discrete frequencies and covering all directions of geographical space. This leads to the calculation of a 2D periodogram (C) or spectral density of the SRTM image window (Stoica and Moses, 2005) by taking the modulus of the Fourier coefficients yielded by the Fast Fourier Transform. The window mean elevation is subtracted before applying the 2D DFT (technically, the central cell of the periodogram of "zero frequency" is set to zero). Furthermore, periodogram entries are rescaled through dividing by the total variance of grey levels (i.e., elevation here) in the image window (Couteron, 2002) as to make periodogram values (or 'entries') portions of the total window variance. Equivalently, the periodogram can be obtained by taking the Fourier transform of the autocovariance function of the image grey level values (Stoica and Moses, 2005) before dividing by total variance as to decompose the autocorrelation function with respect to spatial frequencies. Autocovariance is a central structure function for signals. It is closely linked to the semivariogram, which has been used in geomorphometry to define texture features (Balaguer et al., 2010). Both methods belong to the 'statistical approach' to texture (Haralick et al., 1973) that directly processes grey level variations without any prerequisite of identifying objects.

FOTO then summarizes the 2D periodogram by calculating an r-spectrum (D) giving the azimuthally averaged proportions of variance explained by successive harmonic spatial frequencies r (expressed in cycle/km) irrespective of geographic directions (Mugglestone and Renshaw, 1998). This simplification from 2D periodogram to 1D r-spectra means renouncing to the information relating to possible main orientations or quantifying the magnitude of anisotropy, which is accessible from the 2D periodogram (Mugglestone and Renshaw, 1998). We shall show hereafter that the information contained in the variation of a very large number of r-spectra over a broad territory is, however, interesting for geomorphic mapping. But we agree that periodogram features linked to orientations and magnitudes thereof would be worth considering for future refined applications. Once computed, r-spectra values are assembled in a matrix for which windows are rows and harmonic spatial frequencies are columns. Each cell of the matrix expresses the portion of window variance accounted for by a given spatial frequency. On this matrix we performed a standardized principal component analysis (PCA) (Manly, 2004) in order to compare the texture of a very large number of windows (here an order of tens of thousands of them) on the basis of the associated r-spectra (Couteron, 2002).

The PCA is a statistical treatment for representing a data set with several inter-correlated quantitative variables in a reduced dimensional space. New uncorrelated variables (principal components or "axes") are linear combinations of initial variables. The first component is the linear combination of the initial variables, which represents the maximum variance. The successive components are orthogonally built and account for shares of residual variance of decreasing importance. In FOTO, PCA orders windows along texture gradients. Generally, the first axis opposes the coarsest textures (i.e., patterns, reproducing themselves one or two times within the reference windows) to fine textures (reproducing themselves many times), while the second axis often opposes intermediate textures to heterogeneous patterns involving coarse and fine textures (Couteron et al., 2006). We expect windows located around the origin of the axes to display a mix of different types of texture (textural heterogeneity). Absence of periodicity in the image window would result in a very prominent first axis. The size of the analysis window determines the scale of analysis and therefore the actual resolution of the output textural map.

By changing window size, the FOTO method allows for multiple-scale analyses with the same initial data (here SRTM elevation image). In addition to window size, using overlapping sliding windows allows increasing the nominal output resolution (i.e., distance between the centers of two successive overlapping windows). As already observed (Couteron et al., 2006), texture gradients provided by FOTO change progressively with window size, and complementary information is to be expected only when using contrasted sizes. As landform sizes

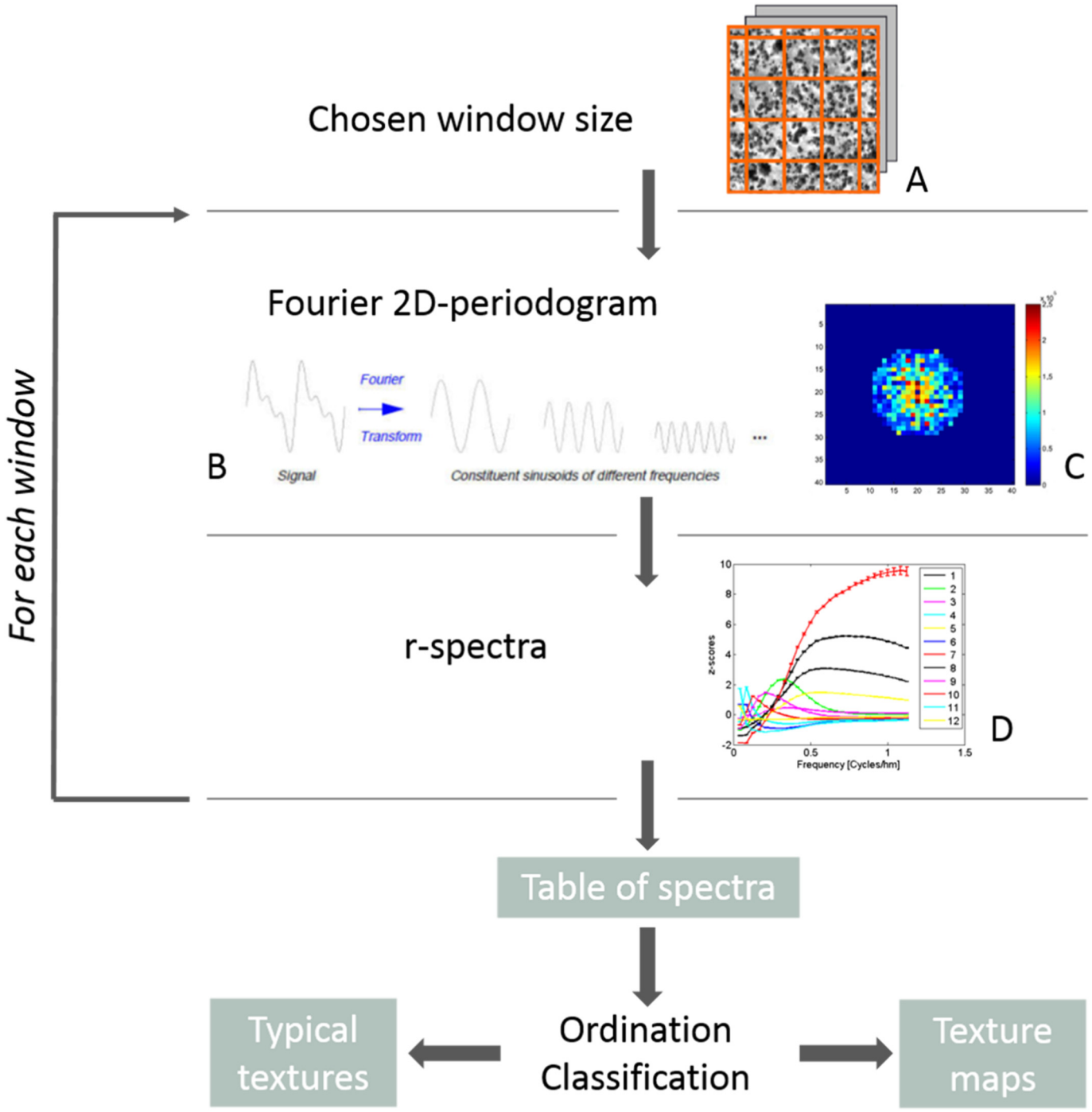

Fig. 2. The steps of textural analysis with FOTO. (A) Process starts with subdivision of the analyzed image into square windows; (B) decomposition of signal at window scale by 2D Fourier transform; (C) 2D Fourier periodogram; (D) examples of r-spectra giving the proportion of variance explained by harmonic spatial frequencies for some hypothetical classes of texture.

may be very variable and we are interested in landforms of 100 m to 10 km, we have done dozens of tests with different scales (i.e., different sizes of windows, from 300 ∗ 300 m to 15 ∗ 15 km). We used the existing work on landform delineation carried out in French Guiana (Guitet et al., 2013) to get preliminary information of the ranges of sizes displayed by landforms in the Eastern Guiana Shield. From these preliminary trials, we selected one reference output resolution (of 900 m between centers of sliding windows, which is a multiple of the SRTM resolution) and three scales of analysis corresponding to window sizes 2.4 × 2.4 km, 6 × 6 km, and 9 × 9 km. Through preliminary tests, this set of sizes proved to be efficient for distinguishing the different types of 'landforms' that were previously identified in French Guiana by Guitet et al. (2013) and for highlighting similar landform shapes and repetition thereof. The smallest scale of 2.4 km provides accurate characterization for the repetition of small landforms (i.e., from 100 m to the kilometer-like hills or inselbergs, for example), while larger scales help to distinguish among larger landforms, as mountains or large plateaus. We retained the three main PCA axes obtained at each scale (window size) as new variables that summarize textural variation. These axes explained at least 85% of the total variance of each of the three scale-specific analyses (see the Results section, below).

On the basis of this set of nine axes, we then performed a general ordination of landform types that we called 'General Textural PCA' (GT-PCA in the sequel) for having an overview of the multiscale textural

variability. However, this ordination cannot make a distinction between areas showing different ranges of elevation, slopes, and convexity while displaying similar texture (see illustration in Fig. 3). Indeed, FOTO-based textural analysis is a decomposition of the spatial autocorrelation function (i.e., variation of relative elevation, Table 1). By design, it does not take into account the absolute elevation or its range of variation (local relief) as to decouple the study of 2D spatial variations from their grey level scaling. This decoupling, which we initially adopted to get robustness against instrumental artifacts of grey levels in air photographs (Couteron, 2002), echoes a classical distinction in geomorphology between descriptors of vertical (relief) and horizontal (texture/grain) variations (Mark, 1975). FOTO is implementable via a program provided by N. Barbier that was compiled from Matlab® (The Mathworks Inc.) functions (written by N. Barbier and P. Couteron). The program uses geotiff format images and yields the matrix of r-spectra as well as maps of window scores along the three main PCA axes (geotiff format), which show texture variations.

Hence, in a second step, we used physiographic criteria derived from SRTM in addition to textural signatures. The criteria selected for this step and computed at 900 m resolution are presented in Table 1. Some of them are straightforward (mean altitude) or have been defined in previous papers (dissection, convexity, wetness). We also considered the relative extents of gentle and steep slopes. By using all these criteria, our aim was to assess the complementarity with textural signatures and express synergies between both systems in order to reach a more relevant classification and mapping of landform types. For this, we run a Global PCA (G-PCA in the sequel) with the 9 texture axes and the 6 physiographic criteria (Table 1) as input variables. We pursued by a classification with 900 m as common output resolution using the K-means method (Manly, 2004) implemented in R (packages ade4 - Dray et al., 2016, and raster – Hijmans, 2016; R Core Team, 2017). The classification was parameterized to provide 16 classes. This number was chosen with the aim to cover the 12 landscape classes defined in French Guiana from Guitet et al. (2013) with four additional classes that were not observed in French Guiana though supposed to exist in Amapa, especially near the Amazon mouth (Bizzi et al., 2001; Jardim et al., 2015).

2.4. From landform types to landscape unit mapping

To increase the legibility of the final map, we chose to aggregate the landform types, which were sufficiently similar in terms of geomorphic characteristics (i.e., texture plus physiographic criteria) while being frequently contiguous in the map of landform types. To measure contiguity (Vogt et al., 2007), we counted the perimeter pixels between each pair of types as to build a contiguity matrix (Saerens et al., 2005), which was analyzed as to emphasize the groups of landform types that were the most frequently contiguous (see Appendix B for methodological details). We principally considered the geomorphic similarity as per the final G-PCA and ensuing k-means clustering (Fig.7) to decide whether to regroup or not. We then referred to the contiguity analysis to understand to what extent the regrouping of landform types into landscape units is improving the legibility of the map and how it can be interpreted from a geomorphological point of view (Appendix B).

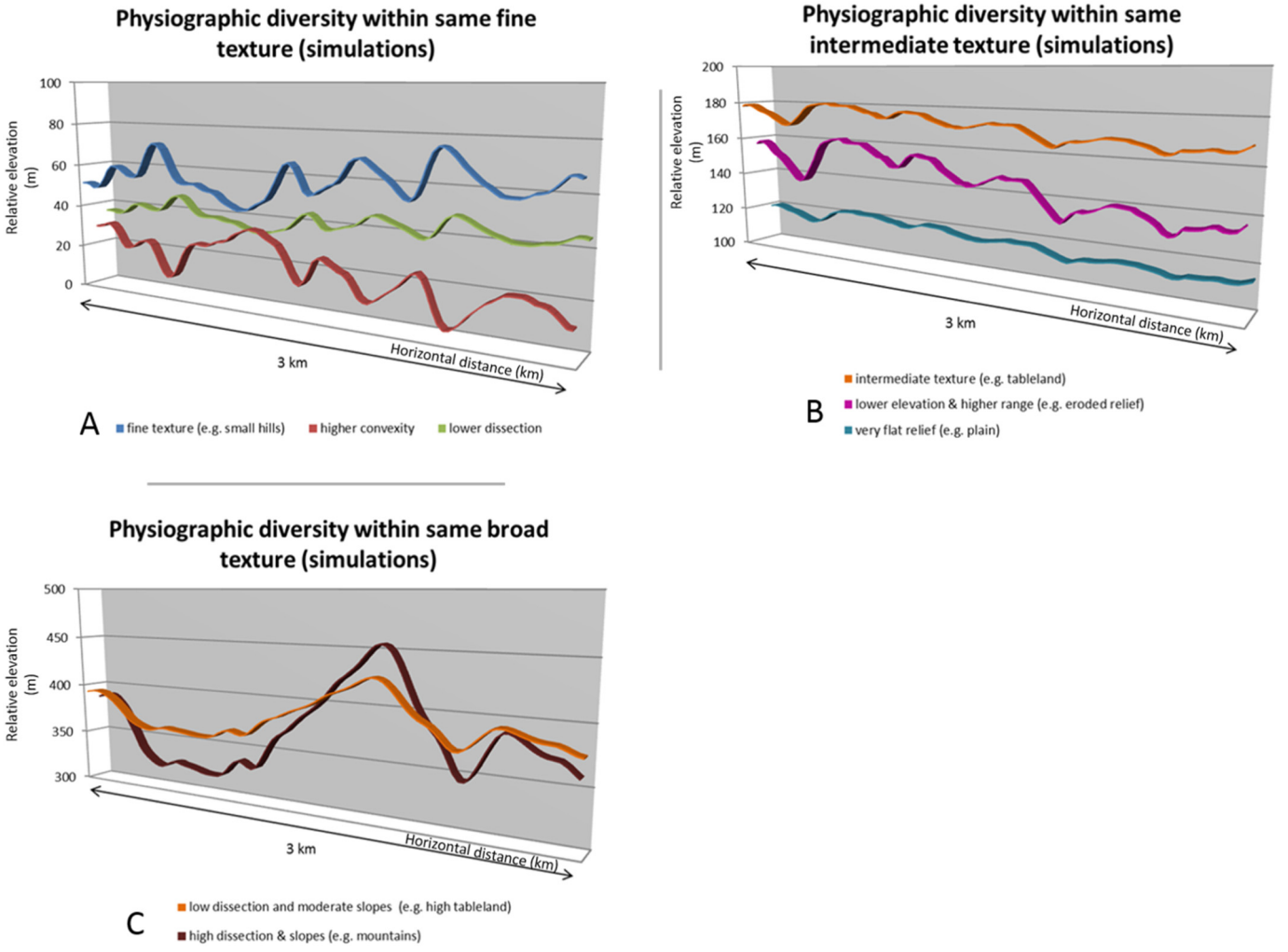

Fig. 3. Illustration from arbitrary idealized elevation profiles of possible physiographic diversity in the classes of fine (A), intermediate (B), and coarse (C) textures. Profiles display very similar textures in spite of variation in physiographic features such as depth of dissection, elevation, or convexity.

Table 1
Presentation of physiographic criteria and underlying relief properties.

Criteria	Factor	Computation	Reference
Dissection	Relative elevation range	(Max elevation - min elevation)/mean elevation	Modified from: Nir, 1957 and Jaeger et al., 2008
Altitude	Mean elevation	Mean value at 900 m resolution	
Convexity	Mean convexity	Saga®: Terrain surface convexity	Conrad, 2012
Flatness	Area with gentle slope	Number of pixels with slope <15%	Guitet et al., 2013
Steepness	Area with steep slope	Number of pixels with slope >30%	Guitet et al., 2013
Wetness	Height Above Nearest Drainage (HAND)	Number of pixels with HAND ≤2 m	Renno et al., 2008 Nobre et al., 2011 Guitet et al., 2015c

At the end of this process, we obtained eight landscapes units. Workflow in Fig. 4 summarizes all steps of the process presented above.

2.5. Comparing results with available mapping

In the end, we compared our map of landscapes with the map from Guitet et al. (2013, 2015c) in French Guiana, and the map from the Brazilian Institute for Geography and Statistics (IBGE, 2004, 2015) in Amapa.

The IBGE put online a more recent version of this map (IBGE, 2015) having the same geomorphological units and associated boundaries in spite of change in some unit names. This 2015 version has increased resolution thanks to simple resampling and a nominal scale of 1:250,000. We used this one for our comparison in order to benefit from a better resolution. Comparisons are presented in Appendix C, where more information on the two external maps is also provided. Notablys that these two maps are based on very different premises and do not ensure any consistency of the mapping between the two territories of French Guiana and Amapa, which is among the rationales of the present project. In French Guiana, Guitet's map is derived from SRTM elevation; while in Amapa, the IBGE map is an expert-based interpretation on a set of Landsat (Thematic Mapper – TM, and Enhanced Thematic Mapper – ETM) images and SRTM data, featuring limits of relief units resulting from analysis of roughness of terrain. The IBGE Amapa sheet is, moreover, just a fraction of a large map covering the whole Brazilian Amazon region and which ontology has been designed at this very broad scale (1: 750,000). The quantitative comparison of our mapping with these two independent preexisting maps is not to be seen as a validation process. It is rather a way to identify advantages and drawbacks of our automated method by analyzing to what extent we detect and map the geomorphic structures that have been emphasized by previous maps and to what extent we may be able to go beyond some possible limitations of the existing maps (especially in Amapa).

Information from some of the authors of this paper, based on their field experience, direct observations (VDS, SG), and earlier publications was also used to analyze and assess the different results and provide interpretations.

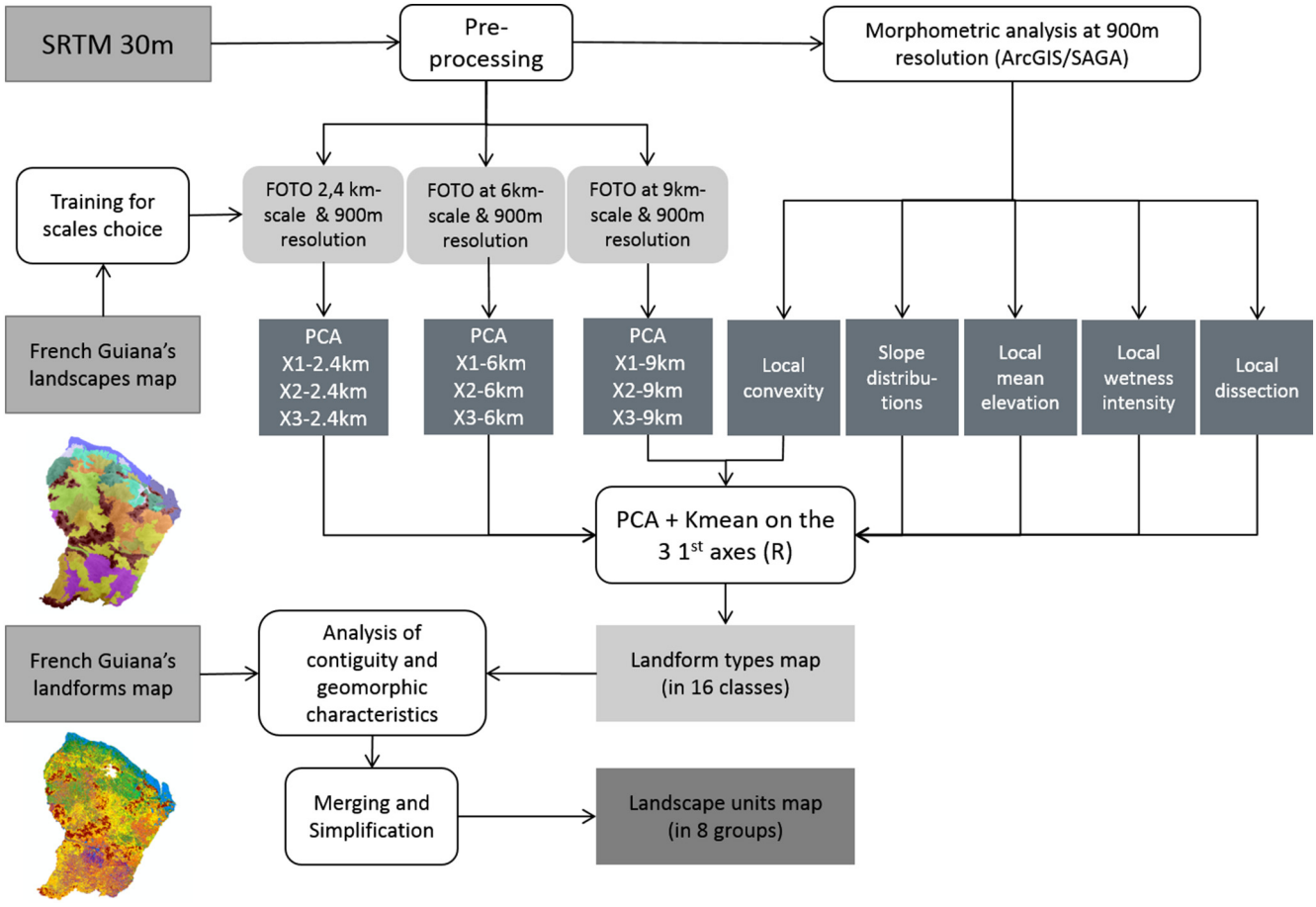

Fig. 4. Workflow of the study. SRTM 30 m is used to make a textural analysis using the FOTO algorithm. Synthetic textural variables (i.e., main PCA axes at different scales) are then analyzed with physiographic criteria to build and interpret a map with 16 classes of landform types with post-hoc clustering in eight landscape units.

3. Results and interpretation

3.1. Textural approach

The correlation circle in Fig. 5 represents the first and second axes of GT-PCA that synthesized the main textural gradients yielded by the textural analyses at multiple scales (windows of 2.4, 6, and 9 km; see also Appendix A). This GT-PCA yielded three first axes representing respectively 33%, 25%, and 20% of total variance of the scale-specific main textural gradients. Axis 1 (horizontal) is mainly built by first and second axes of all the three FOTO scales (with a maximum correlation relating to axis 1 at 9-km scale and axis 2 at 2.4-km scale). Axis 2 (vertical) of GT-PCA mainly depends on the third axes of all three FOTO resolutions and, in smaller proportion, on axis 2 from scales 9 and 6 km. Last, axis 3 of GT-PCA (see Appendix A) is mostly composed by axes 1 from scale 2.4 km and 6 km. The correlation circles of the GT-PCA showed that the analogous axes of the three initial scale-dependent FOTO PCAs were generally intercorrelated, thereby pointing toward geomorphic patterns of fairly similar characteristic scales (about 200 m for axis 1 and >700 m for axis 2). This structure was very strong regarding the batches made of the second axes of the scale-specific FOTO PCAs (Fig. 5, along the horizontal axis) and the batch made of the third axis of FOTO PCAs (Fig. 5, along the vertical axis). The first axes proved less intercorrelated; and this can be explained because, while extending the window size, some new types of geomorphic patterns are integrated in the FOTO analysis. We note that the axes provided by the 6-km window logically had an intermediate position among the analogous axes.

The interpretation can be carried out further when plotting all the windows along the GT-PCA axes and when extracting pictures of the most typical windows and texture types across the scatter plot (Fig. 5). Pictures used in Fig. 5 to interpret axes are 9 km wide. Axis 1 proved to be relevant to measure textural grain (coarser side negative, finer side positive). Position along axis 2 corresponded to grain regularity with more homogeneity (dominated by intermediate textures) for strongly negative values and more heterogeneity for positive values. The definition of axis 3 (not shown in Fig. 5) is more abstract in terms of geomorphological analysis and corresponds rather to the statistical refinement of the trends depicted by the previous axes.

The map on the right side of Fig. 5 is built on the three first PCA axes coded in Red Green Blue (similarly to the window cloud overlaid on the correlation circle). This map of the GT-PCA scores suggests the existence of characteristic areas by color aspects. It exposes large areas with flat relief in grey (i.e., very small values on all three axes) that correspond to plains (window with coordinates 0 0 0 is typical). Regions in cyan have positive values on axis 2 and negative on axis 1 (as for the illustrating window with coordinates −2, 4, 1) corresponding to very smooth albeit ample reliefs (among which are mountains and large valleys) whose size by far exceeds that of the analysis windows. At the upper right part, regions in pale yellow with positive values on axis 1 and on

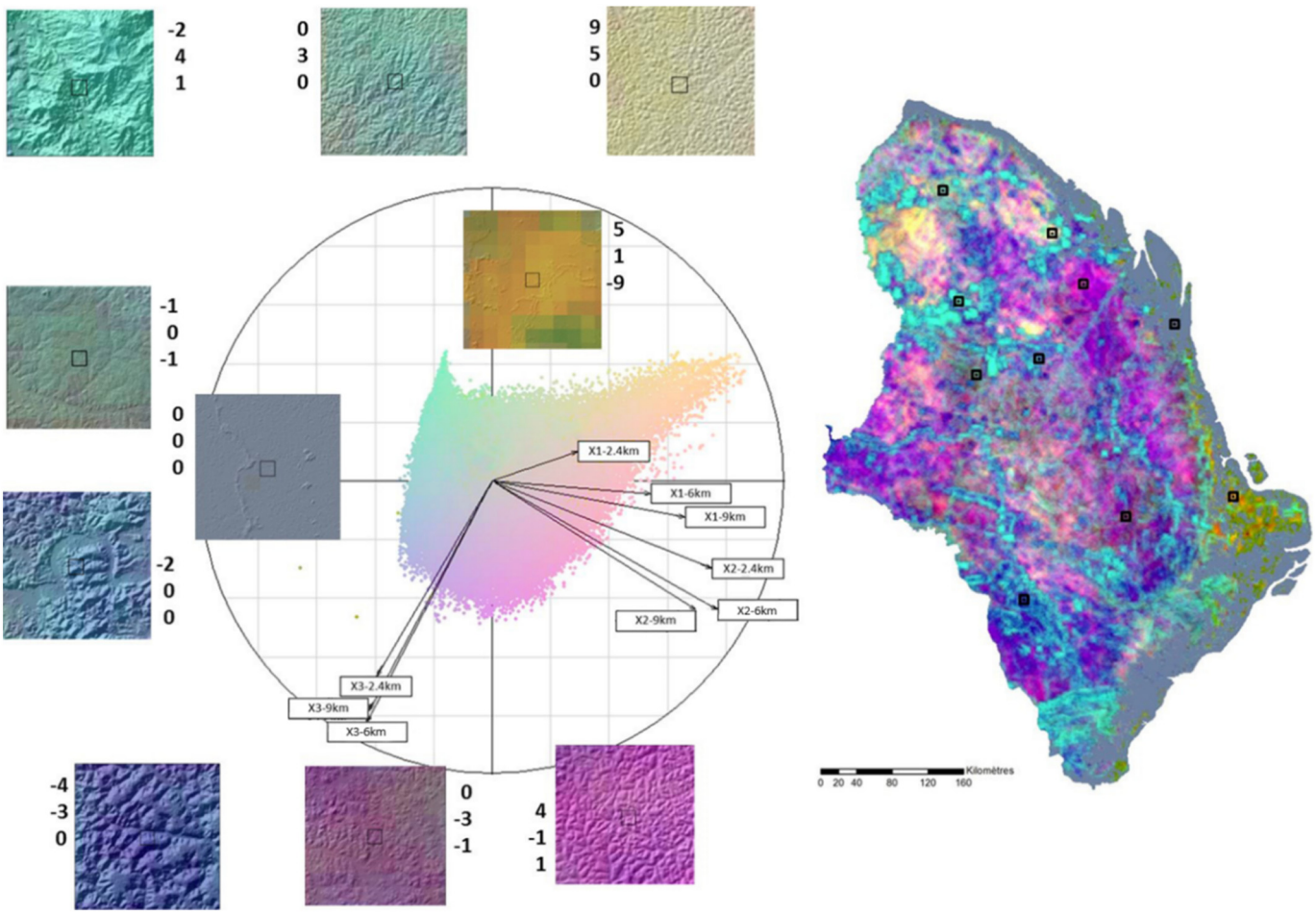

Fig. 5. Correlation circle for the two first axes of the general textural PCA (GT-PCA, left) and associated map of PCA scores (right). The overall cloud of windows is superposed to the correlation circle. Large images encompassing 9-km windows selected for illustration sake (symbolized in the map by a small black square) are displayed and associated figures are the scores on PCA axes of the reference windows (axis 1 then axis 2 and axis 3, respectively). The variables (arrows) are axes of the scale-specific PCA with labels mentioning axis number (×1, ×2, or ×3) and window sizes (2.4, 6, or 9 km). Right part, map of GT-PCA results where the scores along the three first axes (compiling 9 axes of 3 initial PCA using different window sizes) are displayed as an RGB (Red-Green-Blue color coding system) colored composition.

axis 2 correspond to very small and similarly shaped reliefs repeated many times in the analysis windows. We also observed size gradient leading from small to larger landforms (in pink and purple, respectively) having both diversified shapes. The first extremity of this gradient corresponds to positive values on axis 1 and negative ones on axis 2 with an illustrating window having coordinates (4, −1, 1). The opposed extremity pertains to negative values on both axes, e.g., window (−4, −3, 0). Between clusters presented above, intermediate areas colored in pale pink/purple/blue, according to variation of window scores along axes 1 and 2 (pictures on bottom right) show more complex, often heterogeneous topographic features. Inside the coastal plains, some inclusions of bright colored areas (yellow, light green, and orange) are present and indicate strongly negative values on axis 3 (illustrated by window with coordinates 5, 1, −9), which corresponds to strong variability in the vegetation cover.

3.2. Integrating physiographic criteria to texture

In a second step, we mix the nine scale-specific FOTO axes with the physiographic criteria (i.e., Table 1) to carry out a G-PCA. Eigenvalues (Fig. 7) of the three first axes reached respectively 26%, 20%, and 15% accounting for a total of 60% of variance. On the correlation circle for the first two axes (Fig. 7), we note that axis 1 is mainly composed by elevation, steep slope fraction ('Steepness'), and convexity on the negative side, opposed to wetness, low slope fraction ('Flatness') and to the first axis of FOTO at the smaller scale (2.4 km). The second axis is built by axis 2 of FOTO at all scales. Overall, physiographic criteria are mainly related to axis 1, whereas textural features are more correlated with axis 2, suggesting strong complementarity between the two sets of geomorphic features. Moreover, physiographic criteria allowed for making a better distinction between some clusters that present quite similar textures but correspond to different kinds of flat reliefs (e.g., within low plains in grey or within high eroded tablelands in blue in Fig. 5).

The 16 landform classes requested through the K-means classification on G-PCA coordinates allowed for interpreting the triangular shape of the windows cloud by referring to mean values of the criteria (Table 2) and to the average r-spectra of the classes (Fig. 6, computed for the 6-km window).

The color chart in Fig. 7 and Table 2 highlights geomorphic similarity between classes as a basis for grouping them into landscape units. Classes 3, 5, 8, and 11 (negative part of axis 1) correspond to the highest reliefs also characterized by steepness and convexity (Table 2) along with heterogeneous texture at the scale of the windows used for analysis (technically it means a nonstationary signal). The associated mean r-spectra showed a fairly linear shape (with log-log scaling) for high frequency but also featured a rapid decline for large spatial frequencies (above 2–3 cycles/km) (Fig. 6). In Table 2, classes 3 and 5 are characterized by high relief (mean of 260 m asl) with many steep slopes (mean of 23%) and very high dissection (>140 m of amplitude) and were classified as mountains. Classes 8 and 11 are less specific in terms of slope (mean of 16%), while displaying intermediate wetness (23 m of HAND), high elevation (close to 200 m) and also high dissection (close to 85 m) characteristic of mountains. Those classes of strong relief were opposed along axis 1 to classes 15, 14, and 2 relating to the flattest reliefs experiencing the wettest conditions that exhibited rapidly declining spectra suggesting particular weakness of fine-grained patterns. Classes 14 and 15 are very wet plains because they showed high wetness (low HAND values <1 m), with lots of areas prone to flooding. Relief is extremely flat (mean slope of 1.5%) and altitude close to sea level. Class 2 is made of very flat plains, with small elevation (mean of 20 m), very flat relief (2% of mean slopes), and high wetness (HAND about 2 m). The remaining classes located around the origin of the two axes are either of low specificity with intermediate characteristics (classes 12, 13, and 16) or embodying transitions (classes 1 and 7) between the aforementioned three main relief types. Classes 9, 4, and 1 are related to irregular relief influenced by dissection that induces heterogeneous texture often observed at intermediate elevation. Class 7 is interpreted as plains with residual reliefs (like former inselbergs or hills), while the overall relief is much attenuated (mean slopes of 6%) but with locally small places of higher elevation. In the coastal plain in the Amazon mouth, it is referred to as terraces (IBGE, 2015). That class also displays low convexity and dissection that induce pronounced wetness (low HAND, about 7 m, see Table 2). It makes the geographic interfaces with classes 14, 15, and 2. Classes 6, 4, 10, and 9 marked the negative part of axis 2 corresponding to the finest and most regular relief textures. In Fig. 6, the average spectra of these classes show a characteristic shape with a levelling off for intermediate frequencies (between 1 and 2 cycles·km^{-1}) before a rapid dwindling of the spectra for higher frequencies. In Table 2, classes 6 and 10 appear as small reliefs with few steep slopes (about 10%), average altitude of 120 m and moderate dissection (about 45 m) that appears like a succession of hills.

3.3. Analyzing landscape units

For the sake of legibility and interpretability of the final map, we regrouped the landform types showing sufficient geomorphic similarity (as per the color chart in Fig. 7 and Table 2) into eight landscape units. We used the contiguity analysis developed in Appendix B to assess the relevance of the regrouping process and interpret the spatial distribution of the regrouped landform classes. The interpretation of some landscape units, such as 'Mountains' (classes 3, 5) and 'Very flat plains' (class 2) is straightforward. We chose not to regroup this class 2 with 'Very wet plains' (classes 14 and 15) as these two classes had high

Table 2
Main physiographic characteristics of the 16 types of landform as a basis for the definition and interpretation for the eight landscape units (see last column and color chart). Each landscape units can gather several landform types that share geomorphic characteristics (from texture and from physiographic standpoints, see also Fig. 7) and occur as mosaics in thefield.

Class	COUNT	Convexity		Slope (%)			HAND (m)			Dissection (m)			Elevation (m)			Landscape unit
		MEAN	STD	MEAN	STD	MEDIAN	MEAN	STD	MEDIAN	MEAN	STD	MEDIAN	MEAN	STD	MEDIAN	
3	10474	0,4665	0,0622	25,61	15,07	25	42,45	38,72	33	147,44	44,19	141	288,17	99,17	283	Mountains
5	11982	0,4545	0,0574	20,49	12,9	19	33,93	33,29	25	138,97	54,28	131	235,62	111,9	218	
8	12437	0,4547	0,0599	18,98	11,75	18	26,11	23,8	21	92,31	26,4	88	216,59	86,87	195	High tablelands, steep edges and foothills
11	20030	0,4336	0,06	14,61	10,2	13	19,39	19,23	14	78,18	27,01	75	163,24	71,77	160	
9	16917	0,4454	0,0552	14,69	9,49	14	17,97	15,66	15	60,58	15,46	59	185,49	84,26	158	Tablelands
1	17866	0,4493	0,051	15,63	9,84	15	17,52	15,48	15	65,61	17,36	63	161,35	69,99	151	
4	16166	0,4412	0,0507	13,24	8,67	12	13,73	12,11	12	50,37	12,96	49	171,61	59,93	174	
6	6418	0,4377	0,0508	12,7	8,21	12	11,62	10,24	10	45,66	10,27	44	124,16	42,61	122	Hills
10	18037	0,4069	0,0691	10,12	7,68	9	10,02	9,76	8	43,28	12,92	42	116,7	55,86	109	
16	18231	0,3996	0,0648	8,9	7,04	8	10,71	10,83	8	43,99	16,1	41	158,7	61,05	151	Residual reliefs (eroded tableland)
13	26257	0,4044	0,0586	8,67	6,38	8	9,71	8,94	8	38,5	10,14	37	162,95	66,06	161	
12	14978	0,3816	0,0748	7,68	7,09	6	8,9	10,27	6	44,44	19,84	41	96,54	59,94	85	
7	34852	0,3745	0,0669	6,01	5,49	5	7,07	7,43	5	31,18	11,52	29	77,88	69,97	48	Plains with residual relief
2	29475	0,286	0,0888	2,51	3,42	1	2,27	3,51	1	14,8	7,79	14	18,69	26,53	11	Very flat plains
14	4450	0,2206	0,0985	1,15	1,8	1	0,76	1,4	-	6,4	3,94	5	9,06	6,22	8	Very wet plains (lake areas)
15	639	0,2336	0,0892	0,99	1,48	1	0,57	0,89	-	4,72	1,98	5	7,73	1,37	8	

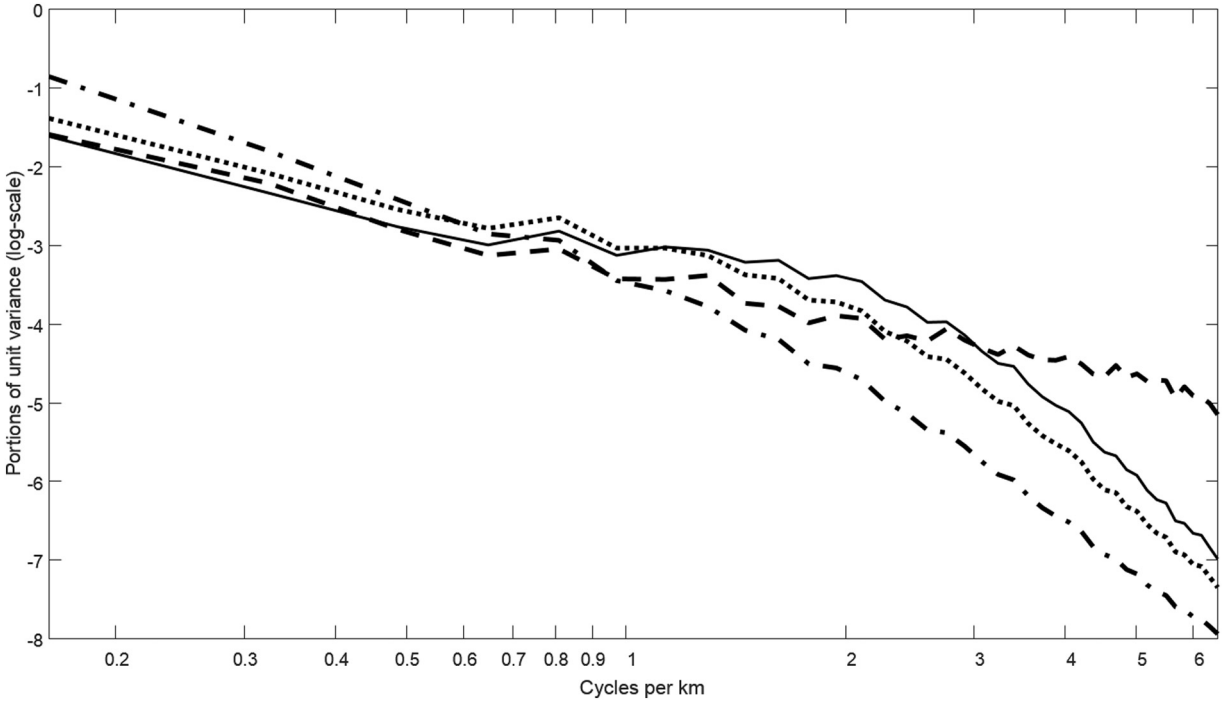

Fig. 6. Average Fourier r-spectra (computed for 6 km wide windows) for major groups of landscape units. Spectra values are rescaled to unity to let the Y-axis express portions of image variance for successive spatial frequencies (abscissa, in cycles/km). Solid line: Hills.Dotted: Mountains/ high-tablelands. Dotted-dashed: Intermediate and transition units. Dashed: flat/wet plains. Only this last group appeared fairly linear in log-log scaling, the other groups displayed a rapid decline for high frequencies above 1 cycle/km (dotted-dashed) or above 2/km (solid, i.e. hills).

contiguity (Appendix B), while displaying geomorphic similarity, large extent (in Amapa), and strong singularity owing to wetness and waterlogging. 'Hills' are also a landscape unit regrouping two classes (6, 10) of peculiar characteristics, notably texture. Hills display a high level of contiguity with the classes regrouped in the "Tablelands" unit (classes 1, 4, and 9). The two classes (8, 11) regrouped as 'High tablelands, steep edges and foothill' rather mark the transition between 'Mountains', and 'Residual reliefs, eroded tablelands'. This latter landscape unit is made of an assembly of landform types (12, 13, and 16) recognized of intermediate characteristics on Fig. 7. The distinction between 'Tablelands' and 'Residual reliefs, eroded tablelands' implies a decrease in average slope (from ca. 15% to 8%), in dissection (from 50–60% to 40%), and in HAND index (from ca. 15 to 10 m) indicating higher wetness (Table 2).

3.4. Comparison with existing map

Detailed analyses underlying these comparisons are presented in Appendix C. The IBGE coverage of Amapa relied on 'formations' that have been defined at the scale of the entire Brazilian Amazon. Most of Amapa was mapped as a single formation of very large extent (60%) called "Convex" relief (IBGE, 2015). Within this area, several classes of our map pertaining to '(High) Tablelands', 'Hill', and 'Residual relief' (Fig. 8) have notable extents, and this geomorphic diversity was not rendered by the IBGE map. Association indices (corrected frequencies) between the dominant IBGE class and our units that overlap with it were overall weak (Table C1 in Appendix C). The second largest IBGE formation was 'Plains' (14% of Amapa, Table C1); and it, logically, yielded strong association with our landscape units 'Very flat plains' and 'Very wet plains'. Plains with lakes were also highly congruent in the two maps. Our unit 'Plains with residual relief' also matched with several IBGE classes that are of limited extent but for 'Tabular' (10.3%). Our 'Mountain' unit showed strong agreement with IBGE formations as 'Pointed' ('*aguçado*') and 'Mountain side'.

The landscape map in French Guiana (Guitet et al., 2013) was closer to our mapping in terms of scale, though it features more landscape units (12 vs. 8 for our map) and the mapping method from SRTM data was different. Table C2 (Appendix C) highlighted a strong agreement of the two maps for the classes related to plains and mountains. Our landscape units relating to hills and tablelands were also congruent with the analogous classes of Guitet et al. (2013). But since our landscape mapping aimed to be more synthetic (less classes for more than twice as large a territory), several of our units displayed strong associations with more than one of Guitet et al.'s (2013) classes (Table C2).

3.5. Overall interpretation of the final map of landscape units

The final map (Fig. 8) of Amapa and French Guiana displays the eight landscape units. It allows a broad scale, overall interpretation of the main geomorphic features of the Eastern Guiana Shield, which were first sketched in Fig. 1. First, the very flat plains (dark blue) are mainly located in eastern Amapa along the coastal line. That landscape unit is also present in small proportion along French Guiana's coasts. Inside this landscape unit, very wet plains corresponded to several lacustrine systems and areas prone to flooding in the southeast Amapa Cabo Norte region (A on Fig. 8). The third landscape unit, i.e., plains with residuals reliefs (light blue), stretch along the coastal line in French Guiana and along the Amazon estuary in the south of Amapa. This unit also encompasses large plains in the center of French Guiana corresponding to the Waki basin (B on Fig. 8). Terrain of this unit is flat overall, but small local relief can be found, like small inselbergs or isolated hills. Some similar plains locally appear in central Amapa. A thin line of this unit is also marking the inland fringe along the very flat plains in Amapa. It makes the transition with eroded tablelands that form our residual reliefs landscape unit (pink in Fig. 8), which is a major geomorphic type in Amapa (consistent with description of Boaventura and Narita, 1974). Indeed, we find eroded tablelands with residual reliefs all over Amapa, especially in the center, north, and west parts where this landscape unit is mixed with the typical tablelands (orange in Fig. 8). It draws a geomorphic continuity between the south of French Guiana and center-west of Amapa on both sides of the Oiapoque valley. In French Guiana, the typical tablelands (in orange) are mainly present in the east and southwest. In association with eroded tablelands (in pink), they form two large areas. The first one extends

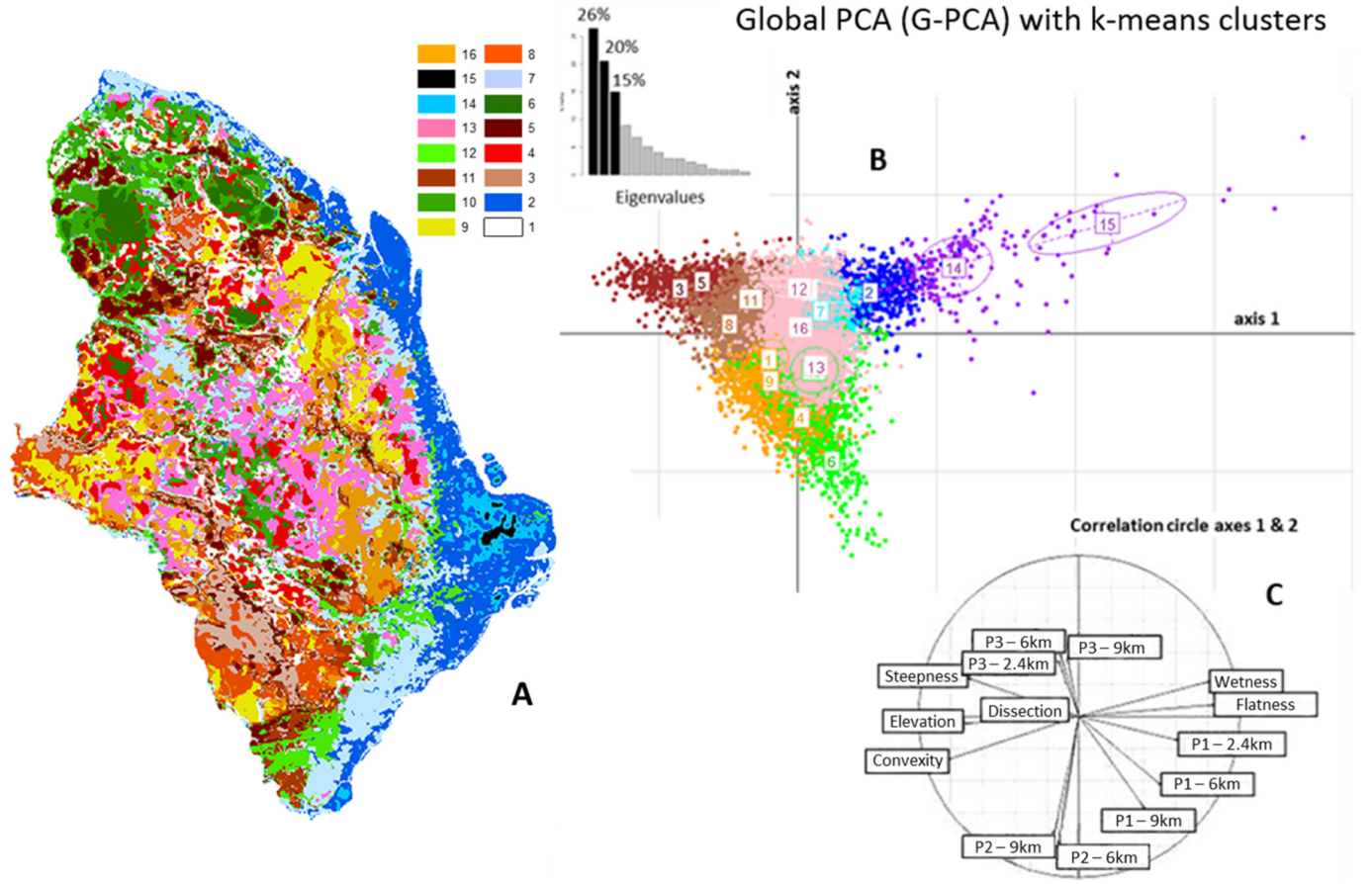

Fig. 7. Results of the G-PCA (integrating textural and physiographic criteria). (A) Map of 16 k-means classes. (B) Axis1-Axis2 plane, with mention of the deriving 16 k-means classes and projection of windows (900-m resolution) along the two first axes. (C) Correlation circle of G-PCA with projection of variables used along the two first axes. The color chart expresses the grouping of landform classes into eight synthetic landscape units.

from the east of French Guiana to the northeast of Amapa along the coastal plain as to mark the dissected edge of the Guiana shield as a transition to the plain with residual reliefs (in light blue). The second one stretches from the south of French Guiana to the west of Amapa around the Tumuc-Humac Mountains (lower zone of the watershed centers). The hills landscape unit (green) is almost exclusively located in French Guiana, more precisely, in the northern half, along the Maroni basin (C on Fig. 8). Small patches of that landscape unit occur in central Amapa. Mountains (dark brown) are regionally organized in three belts (Fig. 1): the first one composes the north synclinorium in French Guiana, and the central one cuts French Guiana in half. The last belt associated with high tablelands ranges compose the border between Amapa and Southern French Guiana (Tumuc-Humac, D on Fig. 8) continuing toward the south of Amapa to include Iratapuru Serra (Fig. 1) before ending with the Amazonian sedimentary basin parallel to Canal do Norte of Amazon River (E on Fig. 8). Another, thinner mountain range (Lombarda Serra, F on Fig. 8, see also Fig. 1) in northern Amapa is oriented from northwest to southeast and is less than half as long as the previous one. Finally, in the center-south of Amapa, a small mountainous landscape unit is identified south of the municipality of Serra do Navio. The last landscape unit (light brown) gathers foothills, steep edges, and high tablelands. It corresponds to areas at the interface between mountains and tablelands or to borders of tablelands cut by deep riverbanks with steep slopes like the Oiapoque River's surroundings (G on Fig. 8). This valley about 3 km in width, incises a large area of eroded tablelands, delineating the eastern border of French Guiana with Brazil. We also note an area of high tablelands (light brown) southwest of Amapa that is distinct from the other tablelands because of the sedimentary nature of the surrounding substrate, which is more erodible than crystalline soils (H on Fig. 8).

4. Discussion

The lack of geomorphic mapping at appropriate scales is a serious limitation for assessing and managing land and resources in the parts of the humid tropics that are sparsely populated. To cope with the shortage of manpower and means, automated or semiautomated processing of freely available digital topographic information is an interesting option that was here tested at the scale of the Eastern part of the Guiana shield (French Guiana and Brazilian State of Amapa).

Using the FOTO algorithm (Couteron et al., 2006), we analyzed the textural information of SRTM with a multiscale approach in order to map geomorphological features at a regional scale. Based on texture indices, we obtained different types of geometric signatures relating to landform types that allowed us to distinguish consistent geomorphic patterns over the study area (Fig. 5). However, our textural approach is principally designed to characterize how variations in elevation are distributed in the horizontal plane, in a way that is fairly decoupled from the amplitudes of these variations. Indeed the FOTO method, through the discrete Fourier transform, is decomposing the spatial autocorrelation (Stoica and Moses, 2005) into spatial frequencies independently of local mean elevation or variance. It is therefore not devised to distinguish between topographic features that show the same patterns of autocorrelation but different absolute values or amplitudes of variation of the signal (i.e., elevation, see Fig. 2). Following an ancient line of thought decoupling 'texture-grain' features from 'relief' amplitude variables (Mark, 1975; Iwahashi and Pike, 2007), we enhanced the textural characterization by adding simple physiographic criteria (mean absolute elevation, mean local elevation, slope distribution, convexity, and wetness indices). They logically proved complementary to synthetic textural variables as they

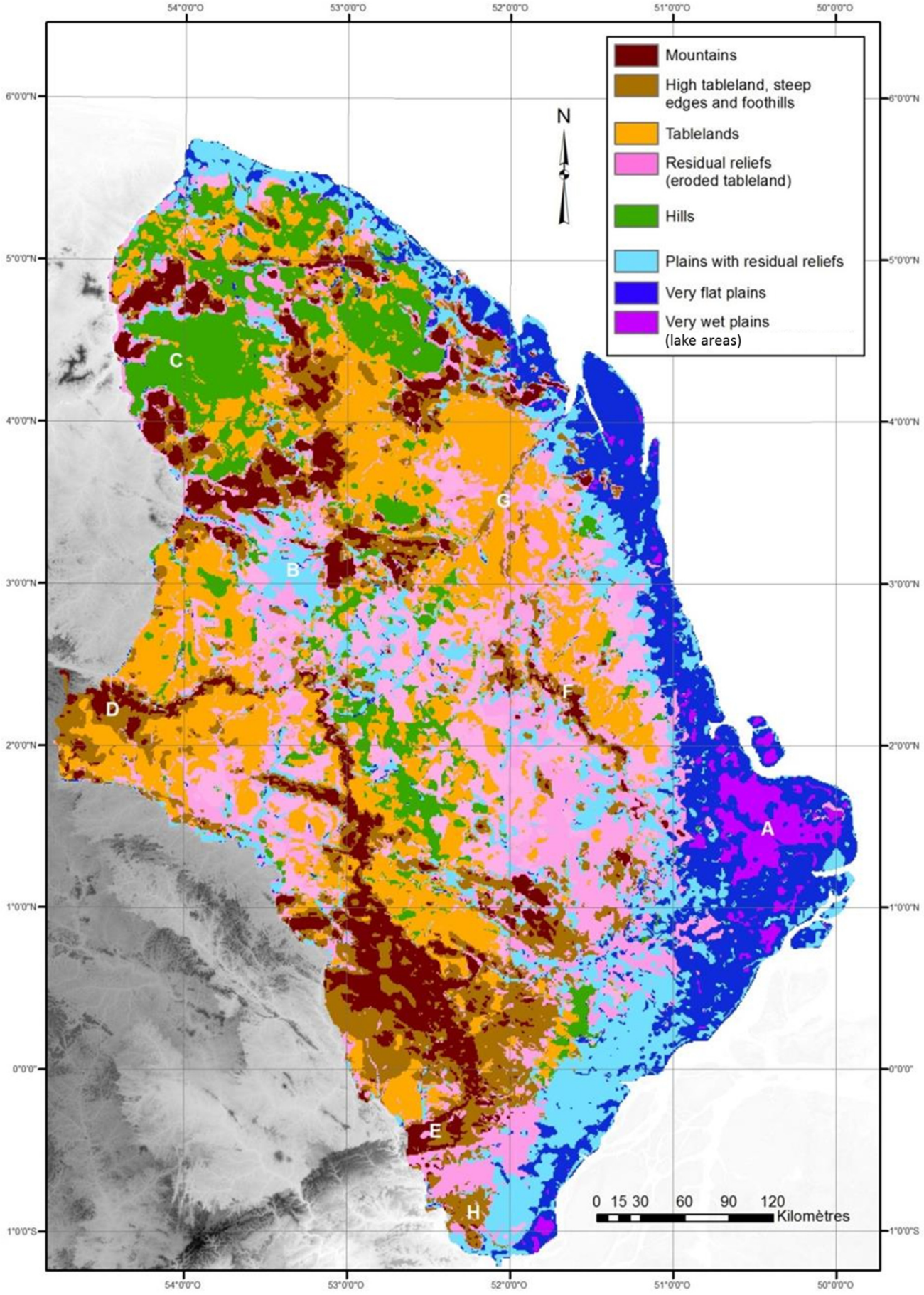
Mountains
High tableland, steep edges and foothills
Tablelands
Residual reliefs (eroded tableland)
Hills
Plains with residual reliefs
Very flat plains
Very wet plains (lake areas)
N
A
B
C
D
E
F
G
H
0 15 30 60 90 120
Kilomètres
54°0'0"O
53°0'0"O
52°0'0"O
51°0'0"O
50°0'0"O
6°0'0"N
5°0'0"N
4°0'0"N
3°0'0"N
2°0'0"N
1°0'0"N
0°0'0"
1°0'0"S

determined a specific PCA axis (axis 1 in Fig. 7). Conversely, successive PCA axes 2 and 3 in Fig. 7 were built from textural features and did not substantially correlate with any of the six physiographic criteria.

We referred to the k-means classes resulting from the overall approach (integrating synthetic texture indices and physiographic criteria, Fig. 7) as "landform types", i.e., 'assemblages of repeating patterns of landform elements with a characteristic pattern and scale of repetition' (MacMillan et al., 2003) with more or less homogeneous elements of various shapes and sizes (indicated by the textural analysis), situated in a specified context (indicated by the physiographic criteria). Taking a leaf from MacMillan et al. (2003), we then moved to a more synthetic upper level 'by agglomerating similar, and adjacent, landform types'. But we referred to them as landscape units instead of 'physiographic types' as did MacMillan et al. (2003) because terminology in the literature is variable and dependent on reference scales and algorithms applied to DEM data (MacMillan et al., 2000; MacMillan and Shary, 2008; Evans, 2012; Guitet et al., 2013). For instance, the data processing scheme applied by Guitet et al. (2013) first identified 224,000 individual elementary landforms (object based-approach from SRTM). Then they were aggregated with substantial expert input for mapping the 12 landscape classes. Our landform types rely on shapes and patterns of repetition of landform and are here identified semiautomatically without delineation of individual landforms, before further aggregation into landscape units. But the comparison for French Guiana (Fig. 9 and appendix C) proved that both approaches yielded consistent results (see below), though our system of eight landscape units (for French Guiana and Amapa) aimed to be more synthetic. For comparison sake, we also used in Amapa a map of geomorphological 'formations' published by the IBGE at the scale of the entire Brazilian Amazonia. This map was built on very different methodological premises compared to the map of French Guiana by Guitet et al. (2013), and we would have faced strong difficulties to draw a synthetic map for the two territories. The mapping we expose in the present paper aimed to fill this gap by implementing a consistent system over the two territories, with potential relevance for a large share of the Guiana shield. Comparing our eight landscape units to the formations of the IBGE maps, we found (Fig. 9, Appendix C) a good agreement for classes relating to plains (nuances of blue) and mountains (nuances of brown). The comparison was, however, limited as IBGE mapped 60% of the Amapean territory in a single formation of 'Convex' relief that overlaps with several of our landscape classes.

Whereas IBGE mapped inland Amapa as a unique and undifferentiated territory, our map shows much more detail, with different landform types (tablelands, foothills, hills, etc.) as evidenced by the reliefs of different dissection. The unit 'High tablelands, foothills, and steep edges' form a typical landscape very specific to, and well developed, in Amapa (particularly in the south). These provide more details around mountains where this landscape unit is mainly located. We also identified hills in the center of Amapa where no reference to them was previously made, at any scale. Finally, very wet areas can be specifically mapped in eastern and southern Amapa. Even though they are well known and already mapped by other techniques (Silva et al., 2006; IRD, 2008; Jardim et al., 2015), they never were automatically mapped at these scales and that resolution.

Our classification allows definition of large regions (formed by repetitions or mosaics of similar relief) but also particular reliefs when they are well differentiated from the surrounding environments. This is illustrated by the zoom box in Fig. 9, which allows us to identify three small mounts around Cayenne city isolated in the largest coastal plains (blue landscape units). Our classification also provides a new picture of transitions between landscape units of large extent, as for tablelands (orange) and residual reliefs (pink).

The contrasts in aims and scales with the maps preexisting in our study area impede us from implementing a rigorous calibration/validation approach, especially in Amapa. Specifically, we had no independent detailed mapping for sufficiently diverse parts of the territory suitable for calibration or validation areas. This situation, however, prevails over most of the humid tropics where regional-scale geomorphic mapping is urgently needed to enhance land planning and natural resource assessment. The comparison we made (Appendix C) allowed us to confirm that the most peculiar structures (mountains, plains) were consistently identified, while for most of inland Amapa, we proposed a more informative mapping than the all-Amazonia ontology of the IBGE map. Obviously, a system designed at larger scale, whatever its merits, is likely to face limitations for downscaling. This also appears for the worldwide precursor works of Iwahashi and Pike's (2007) map that showed little agreement with our mapping as with the previous map of Guitet et al. (2013) (results not shown). Class 9 of Iwahashi and Pike (moderately gentle, fine texture, and high convexity) was dominant for most of our classes as for those in Guitet et al. (2013). Only plains and high reliefs were quite well discriminated by some of Iwahashi and Pike's classes identified via the three variables (slope, convexity, texture) that they relied on for their global classification. Our results suggest that more variables, notably FOTO textural indices, can be useful for classifying geomorphic types at regional scale. Redundancy between geomorphic descriptors, which was pointed out by several authors (Evans, 1972; Iwahashi and Kamiya, 1995) is not a serious problem since multivariate analysis (e.g., PCA) can help produce new synthetic variables that are uncorrelated and efficient for 'general geomorphometry' that is measuring, characterizing, and mapping the continuous variations in a way applicable to any rough surface (Mark, 1975). We also verified that features provided by FOTO clearly relate to texture-grain characterization (sensu Mark, 1975) in a way complementary with physiographic variables that express variations in slopes and elevation and therefore 'relief'. Progress can moreover be expected by using multivariate approaches integrating geographic contiguity constraints so as to directly reach sufficiently compact landform types (Dray and Jombart, 2011) or inversely to understand transitions between types from multivariate descriptors (Couteron and Ollier, 2005). In the present study, we mostly used contiguity analysis (Appendix B) to interpret the spatial distribution of landform types in relation to their regrouping into landscape units, while we based most of the aggregation process on similarity in textural and physiographic variables (Fig. 7). With the aforementioned multivariate methods, contiguity can be directly integrated to the regrouping process. We found several main patterns of contiguity. First, we had straightforward situations where classes having closely related geomorphometric profiles (e.g., classes 14 and 15, and merged in a single landscape unit were frequently contiguous). Second, we noted classes that we did not regrouped in spite of a high level of contiguity and substantial geomorphometric similarity (i.e., very flat plains and very wet plains), mainly because they are of large spatial extent and also because their common boundary marks an interpretable geomorphologic transition. A third situation is made of frequently contiguous classes showing notable geomorphometric differences that were allocated to distinct landscape units. Conversely, some classes of strong geomorphometric similarity were generally not contiguous and showed different patterns of spatial associations with other classes. The 'Eroded tableland' unit provides a good example of this situation. Constituting classes were kept in this unit for simplicity sake, but subtler distinctions could have been made.

Thanks to the rapidity of our semiautomated approach, we reached novel elements of concept concerning large territories that are mostly covered by tropical forests, difficult to access, and where data are faintly available. The approach allows a quick representation of information. The improvement over Iwahashi and Pike's (2007) method by adding a multiscale and comprehensive textural analysis leads to a richer

Fig. 8. Map of eight landscape units (obtained by clustering 16 initial landform types). The initial classes have been delineated by applying the k-means method to textural variables (FOTO method) and physiographic criteria (see text for detailed information). Resolution based on sliding texture window centers 900 m apart.

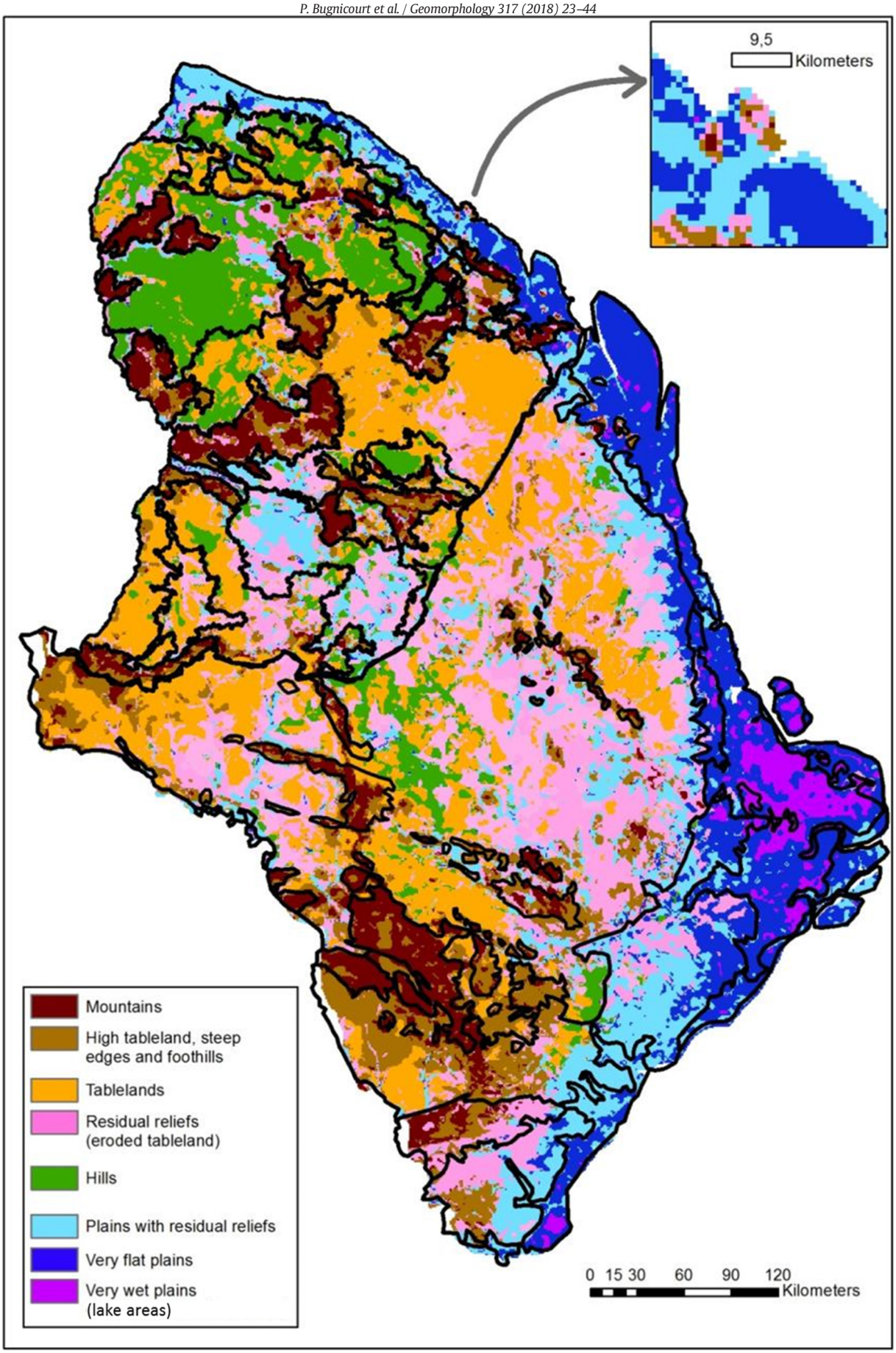

Fig. 9. Superposition on our final map (see Fig. 8) of the boundaries of the published main geomorphological regions (compiled from Guitet et al. (2013) and IBGE (2004)) in French Guiana and Amapa respectively. Based on window centers 900 m apart.

geomorphological characterization, especially in the apparently homogeneous tropical regions. From a practical point of view, applying the FOTO method to SRTM data allowed us to describe the geomorphic context of Amapa and French Guiana in an understandable way for nongeomorphologist end-users of the maps in the fields of land planning and natural resource management. Textural analysis based on 2D discrete Fourier transform proved useful and efficient to define and map geomorphometric features that were not used before. The agreement with existing sources of comparisons, including field experience of some of us, supports the relevance of the approach as does the complementarity with older works (IBGE, 2004, 2015; Iwahashi and Pike, 2007; Guitet et al., 2013). We suggest this approach could be usefully applied for the entire Guiana shield and tested in other contexts following a similar flow of operation provided that the multiscale combination of textural analysis would be adapted and parameterized (through the adjustment of window sizes) to the specificities of each context.

Supplementary Material

Software: the foto.exe program has been created by Nicolas Barbier from earlier functions written by Nicolas Barbier and Pierre Couteron in Matlab® language. It can be run on a Windows 64-byte personal computer and is freely downloadable from http://doi.org/10.5281/zenodo.1216005 or directly requested (nicolas.barbier@ird.fr or pierre.couteron@ird.fr). Maps: digital versions of the Landform types and Landscape units maps presented in this paper are freely available from http://doi.org/10.5281/zenodo.1226381.

Acknowledgements

This paper was principally funded by the BIOMAP project (Guyamazon III program, http://www.guyamazon.org/guyamazon-iii-2015-2018/biomap) with FAPEAP as funder for Brazil and IRD, Cirad, CNRS, Région Guyane for France, and supported by the Observatory of the dynamics of interactions between societies and environment in the Amazon (Odyssea, funding from the European Union's Horizon 2020 Research and innovation program under the Marie Skłodowska- Curie grant agreement No 691053). Synergies from the 3DFORMOD project 'Combining remote sensing and 3D forest modelling to improve tropical forests monitoring of GHG emissions' (EU-H2020 – FACCE ERA-GAS, grant agreement No 696356) are also acknowledged. We thank Dr. Richard A. Marston as editor of this paper along with Dr. Ian S. Evans and three anonymous referees for the thorough and helpful assessment they provided on the first version of this paper. PB performed the analyses during his master's studies and wrote the paper; SG and PC designed the analysis, NB provided a smart version of the FOTO freeware; SG, PC, and VFS supervised the work and participated in writing the successive versions; LB and EDS corrected the final paper.

Appendix A

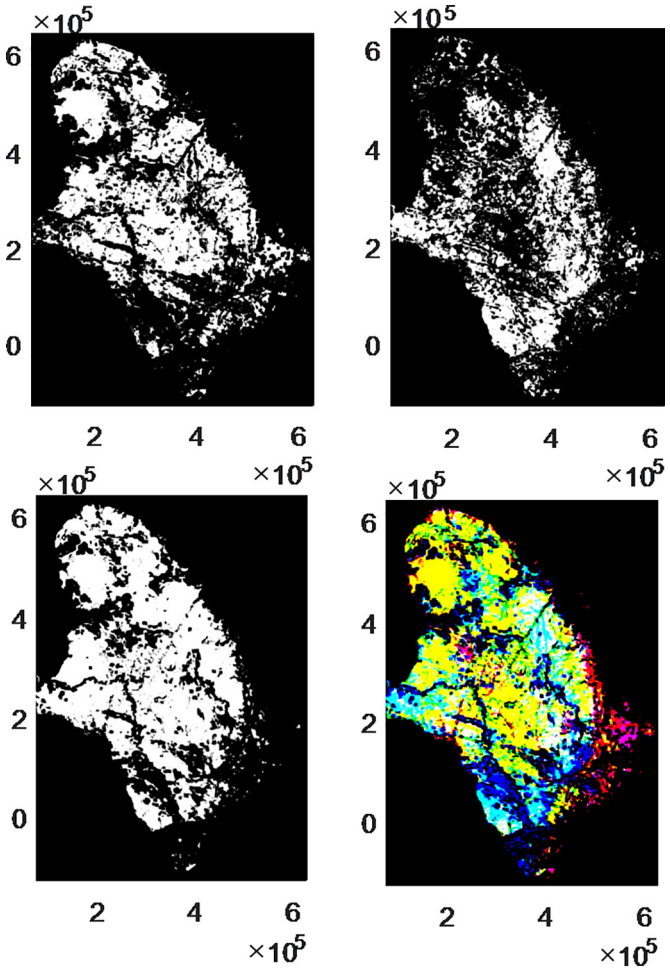

Fig. A1. Maps of windows scores for the three main axes for the PCA used in FOTO for an intermediate window size of 6 km (Axis 1 – top left, Axis 2 – top right, Axis 3 bottom left). The overlaying of the three maps is expressed in Red Green Blue color chart at the bottom right. Map coordinates are in UTM 22 N.

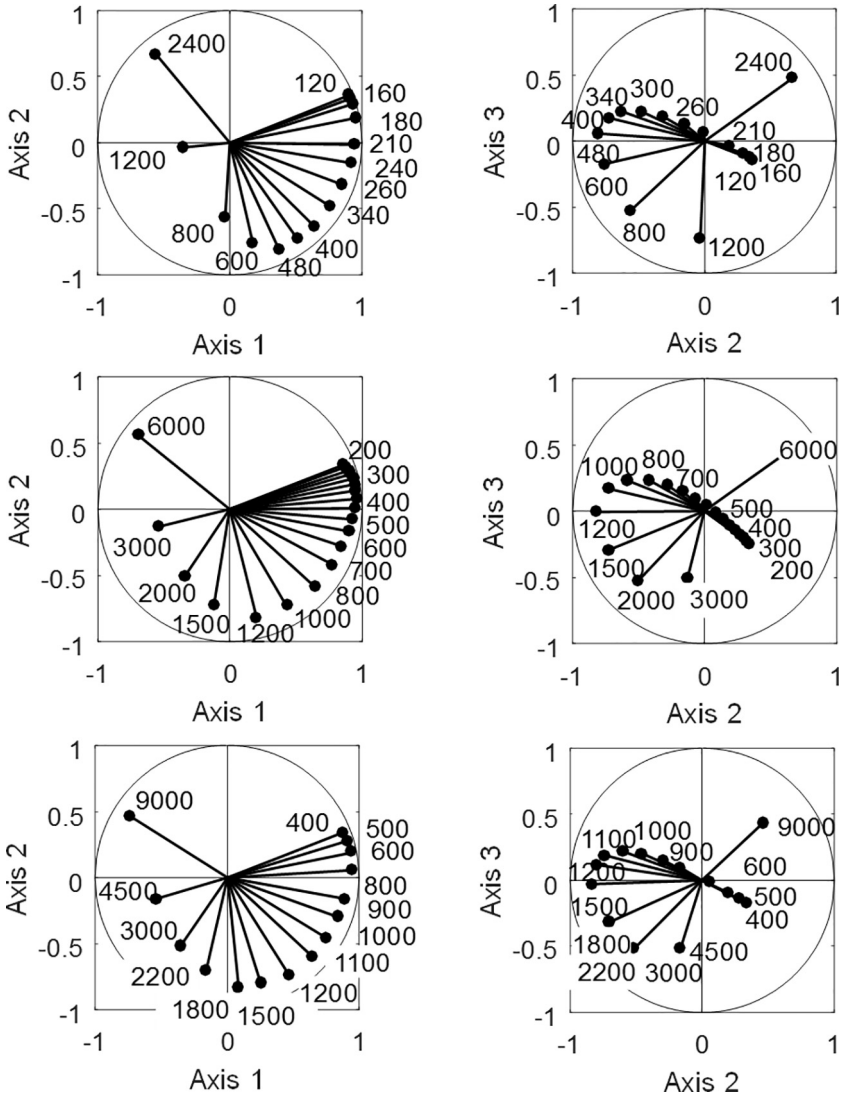

Fig. A2. Correlation circles for the scale-specific PCA analyses used in FOTO for window sizes of 2.4 km (top row), 6 km (intermediate) and 9 km (bottom). The left-side column displays Axes 1 and 2 while Axes 2 and 3 are on the left side. Spatial frequencies are denoted through the corresponding wavelength, in meters. Some values have been omitted to ensure legibility.

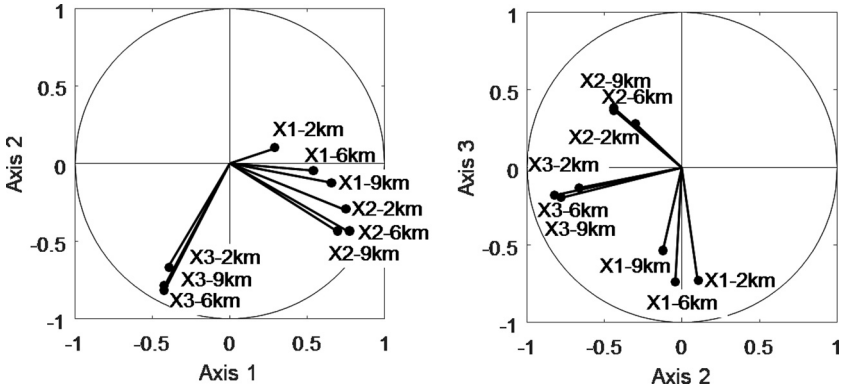

Fig. A3. Correlation circle of the "General Textural PCA" that combined the main textural gradients yielded by the textural analyses at multiple scales (2400 km – denoted 2 km for brevity, 6 km and 9 km). GT-PCA processed the three main PCA axes obtained by FOTO at each of the three scales. Left circle for Axes 1 and 2, as in Fig. 5 of the main text. Right Axes 2 and 3. The variables (arrows) are axes of the scale-specific PCA with labels mentioning axis number (×1, ×2 or ×3) and window sizes (2.4, 6 or 9 km).

Appendix B. Presentation of the 16-class map of landform assemblages and spatial contiguity analysis thereof

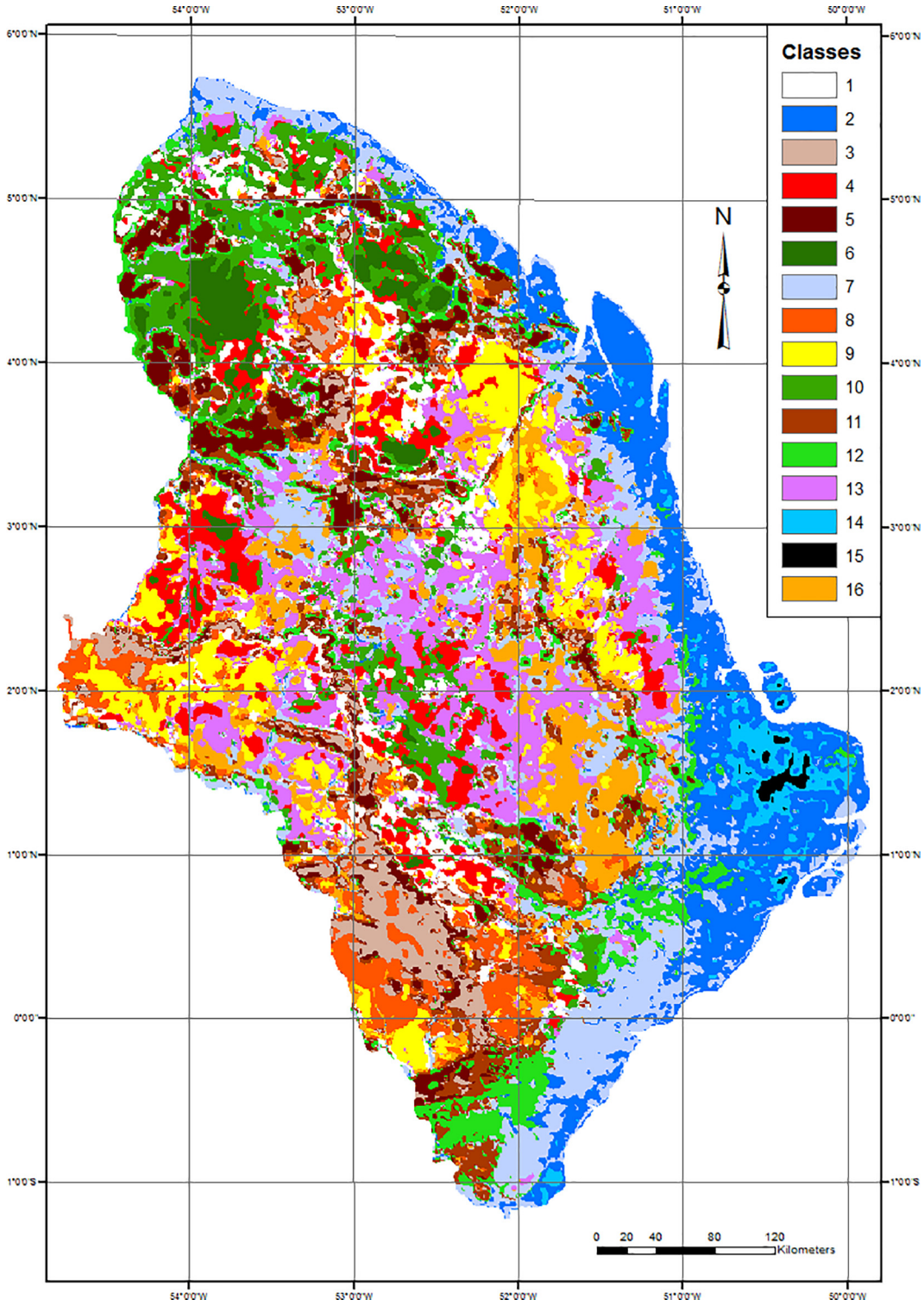

Fig. B1. Geomorphological maps of 16 classes corresponding to landform types. Classes have been delineated by applying the k-means method to textural variables (FOTO method) and physiographic criteria.

Creation of contiguity matrix

The perimeter pixels were identified for each class using basic principles of mathematical morphology. (i) A binary image is first created by affecting "1" values (against "0") to all the pixels of a given class. These pixels are then "dilated" with a "structuring element" (loosely speaking, a neighborhood) with a size of one pixel in each cardinal direction (Vogt et al., 2007). This means that the direct neighbors of these focal class pixels are marked as "1". (ii) The initial binary image is subtracted to the dilated image as to let the resulting binary image features pixels belonging to the "outer" perimeter of the focal class polygons. (These also are "inner perimeter" pixels of the classes neighboring the focal class.) (iii) The outer

perimeter pixels are counted according to the classes to which they belong as to measure the spatial contiguity between the focal class and all the other classes. Classes that are frequently contiguous to each other will tend to share a large proportion of their perimeter pixels. This step is iterated for all the 16 classes thereby providing a "contiguity matrix", M that cross-classifies outer perimeter pixels between the classes.

Let us denote M [mij] the contiguity matrix, which general term mij is the number of class i outer perimeters' pixels belonging to class j and vice versa for mji. Since we are considering outer perimeter pixels, off-diagonal values mij and mji are generally not equal and M is non-symmetric. On-diagonal values are by definition zeros. We compute a symmetric contiguity matrix M_tilde(i,j), as $0.5 * (M + t(M))$, where t(M) is the transpose of matrix M. This step may be seen as averaging outer and inner perimeters' lengths of each class, though the inner perimeters are here implicitly assessed. The off-diagonal values of the M_tilde(i j) symmetric matrix reflect the spatial adjacency of the classes: the higher the values, the longer the perimeters between the classes' polygons. Since all off-diagonal values are positive or null, Mij_tilde is the matrix of a weighted graph (sensu Saerens et al., 2005).

To analyze the contiguity matrix and reach clusters of classes showing high levels of spatial contiguity, we refer to the principles exposed in Saerens et al. (2005), for "Principal Components Analysis" (PCA) of a graph matrix. Let D be the diagonal matrix featuring along its diagonal the sum of M columns. A new matrix L is computed as: $L = D - M$. Saerens et al. (2005) showed that the "nodes" of L (here the landform classes) and their relative proximity/distance (with respect to the shared perimeter length criterion) can be directly mapped in a Euclidean space. This space may itself be approximated in a sub-space of reduced dimension by singular values decomposition (also known as diagonalization). This can be done by carrying out a PCA on L, while the most relevant components providing the best approximation are in this case those featuring the lowest, non-zero eigenvalues (Saerens et al., 2005). We applied standardized PCA to the L matrix computed for the 16 landform types. We kept scores along the two components of smallest eigenvalues to carry out hierarchical clustering of the classes (Ward's criterion). All computations needed for the present Appendix were performed using Matlab® with both existing and personal functions.

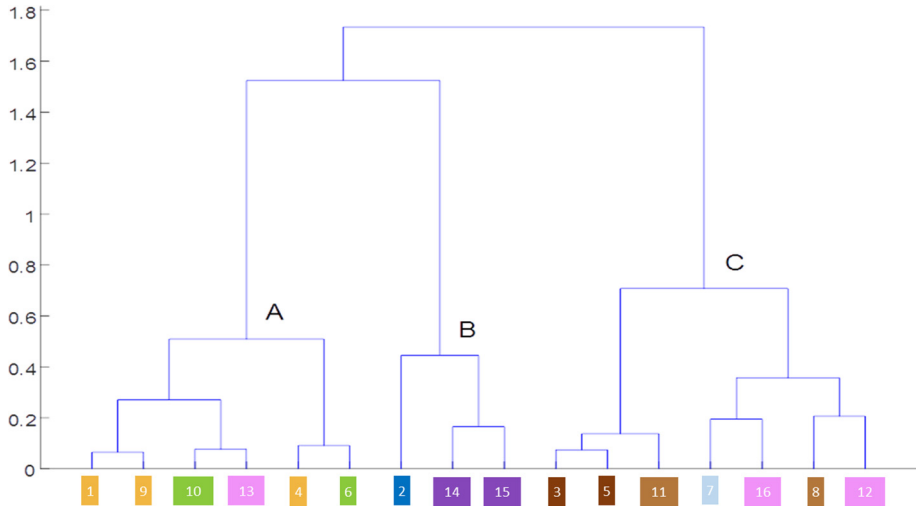

Fig. B2. Hierarchical clustering (Ward's criterion) of the 16 landform types units (numbers along the X-axis) with respect to a contiguity relationship based on shared perimeters lengths: units that are grouped for a low level of variance (bottom of the Y-axis) are those that have polygons sharing the longest common perimeters. Colors indicate the landscape units to which landform classes have been affected (see Fig. 7 and Table 2 in the main text).

The obtained dendrogram (Fig. B2) summarizes the studied contiguity relationship. Landform classes getting grouped near the bottom of the tree are those who are particularly associated in space (see maps of classes). It is specifically interesting to interpret such spatial associations in the light of the geomorphometric similarities which are made apparent by Fig. 7 and Table 2 in the main text, and on which our eight landscape units have been based. The most typical spatial clusters relate to "Mountains" (classes 3 and 5) or to 'Very wet plains' (classes 14 and 15). This second cluster is logically then regrouped with "Very flat plain" (class 2). Two classes imputed to "Tablelands" (1 and 9) also show strong levels of contiguity. We also note clusters expressing spatial contiguity for classes of different geomorphometric profiles and deriving landscape units: 4 and 6 ("Tablelands" and "Hills"), 10 and 13 ("Eroded tableland" and "Hills"), 8 and 12 ("High tableland" and "Eroded tableland"), 7 and 16 ("Plain with residual reliefs" and "Eroded Tableland"). This last cluster is of clear interpretation when considering the eastern fringe of the Guyana shield in Amapa (map on Fig. 5), along which Eroded tableland share extensive borders with Plains with residual reliefs. The previous clusters express subtler spatial associations involving particular classes related to landscape units of large extent (Hills, (High-) tablelands, eroded tablelands). We may note that classes regrouped within these types based on geomorphometric similarity seem to have particular geographic distributions, e.g., for Eroded tableland, class 16 is more in contact with the Plains with residual reliefs while 12 is rather fringing High tablelands, and 13 tends to be adjacent to (Hills) (10). This is interesting to note since the Eroded tablelands landscape unit is simultaneously of large spatial extent and of intermediate geomorphometric characteristics (laying in the middle of Fig.7). At an upper level of the dendrogram (between variance indices of 0.4–0.6, Y-axis on Fig. B2), the classes affected to Eroded tablelands are split between two (A and C) of the main clusters observed at this level (Fig. B2). The left-side one (A) reflects important levels of contiguity between classes pertaining to Hills (class 6 and 10), Tablelands (1,4,9) and Eroded tableland (13). This cluster relates to areas where Hills occur (mainly in French Guiana) and one may note that classes 10 and 13 are frequently separating Hills from Mountains or High tablelands (Fig. 5 map of classes). The constituting classes of these two landscape units (3, 5 and 8, 11, respectively) are indeed part of the right-hand cluster (C) in association with classes 12 and 16 of Eroded tablelands. Cluster (B) is clearly linked to the flattest reliefs.

Appendix C. Comparisons of our landscape units map with some existing mappings

The landscape unit map is presented in Fig. 8 of the main text. It is here compared with the IBGE (2015) map for Amapa and the landscape classes from Guitet et al. (2013) for French Guiana.

1) Objectives and methods

Using Qgis, we overlay the two maps in raster form and generate random sampling points over the area of overlap between the two maps. At each point, category labels are extracted and cross-classified as to create a contingency table between the two maps. Arbitrarily, we assigned rows indexed by i to classes of the focal map and columns (indexed by j) to our landscape units. To ease the analysis of the contingency tables, we computed corrected frequencies, that are fij = n.. ∗ nij/(ni. ∗ n.j), where nij is the number of points classified in cell i,j, ni isthe total number of points relating to class i and vice-versa for n.j. n.. is the total number of points. Corrected frequencies substantially above one indicate a strong association between two categories of the typologies compared. We did not provide test *p*-values since their results depend directly on the number of sampling points used, which is arbitrary.

2) IBGE map of geomorphological formations (in Amapa)

The IBGE map of geomorphological formations covering Amapa is a subpart of a large map covering all Brazilian Amazonia:

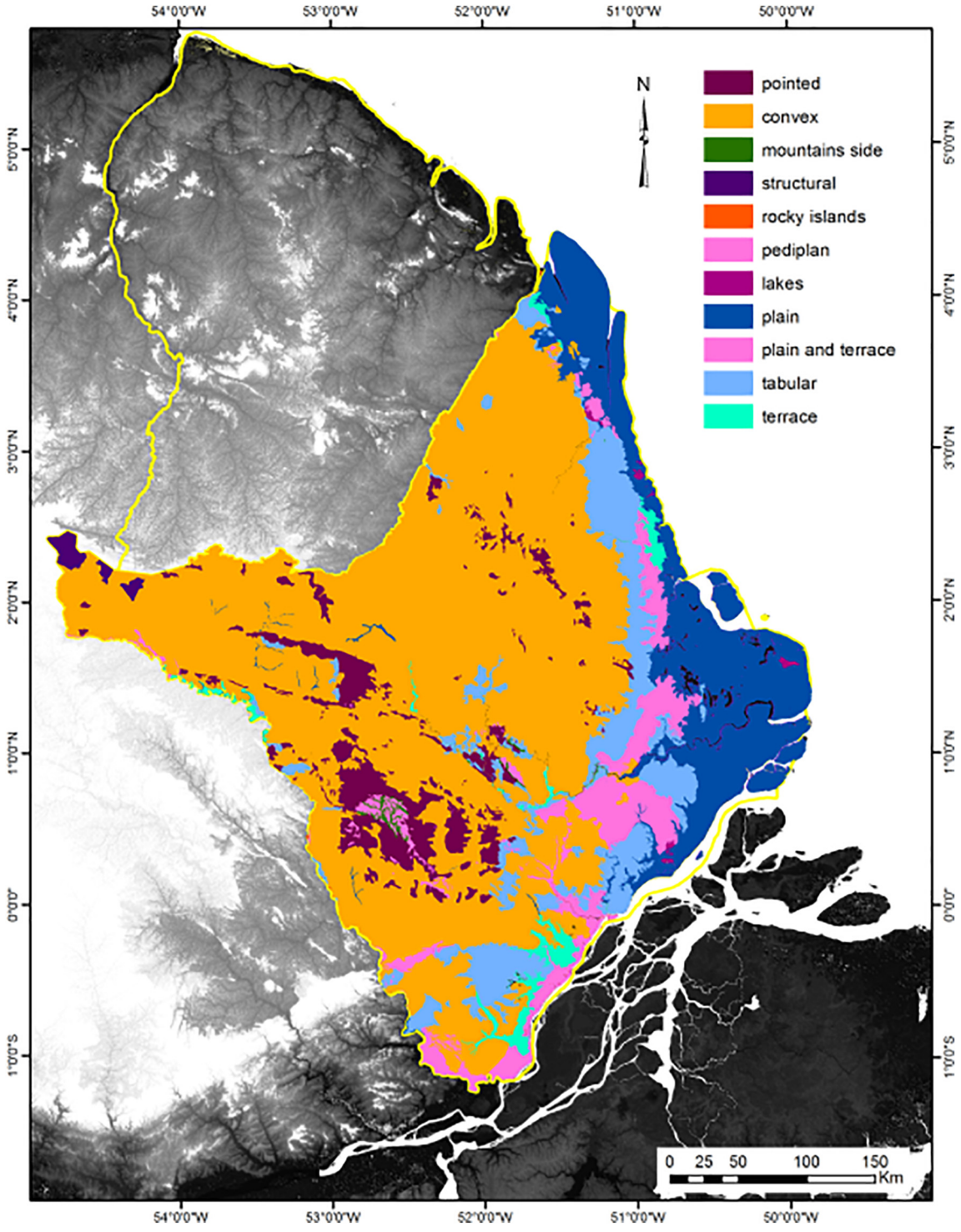

Fig. C1. IBGE (2015) Map of geomorphological formations.

We used a random sampling of 55,000 points over the Amapa part of the study area to compare the IBGE formation map and our landscape unit map. The resulting contingency table featured 38,756 points falling in the area of common validity of the two maps.

Table C1
Cross-classification of 38,756 sampling points between classes of the IBGE geomorphological 'formations' map (rows) and the landscape units (present paper, columns). The last right-hand column and the bottom-row feature the percentages of sampling points in the different rows and columns, respectively. Relative frequencies above 1.5 are highlighted.

		Landscape units (present study)								
		Very wet plains	Very flat plains	Plains with residual	Residual reliefs	Hills	Mountains	High Tablelands	Tablelands	% sampling points
IBGE geomorphic formations		**8**	**1**	**4**	**7**	**6**	**3**	**5**	**2**	
2	Plain	5,97	4,41	0,85	0,05	0,05	0,00	0,01	0,01	14,26
10	Plain with lakes	11,32	3,03	0,83	0,33	0,00	0,00	0,00	0,00	0,15
4	Plain & terrace	2,51	2,46	3,09	0,15	0,59	0,02	0,20	0,01	1,55
5	Terraço	1,21	2,56	3,28	0,15	0,52	0,03	0,15	0,03	1,46
6	Peneplain	1,30	2,39	1,54	0,69	0,23	1,63	0,44	0,00	5,25
3	Tabular	0,05	1,35	2,22	1,32	0,14	0,52	0,52	0,02	10,31
9	Rocky islands	0,00	0,00	0,97	2,71	0,00	0,00	1,07	0,00	0,02
1	Convex	0,00	0,04	0,78	1,33	1,57	0,54	1,26	1,61	60,40
11	Structural	0,00	0,00	0,06	0,07	0,00	8,43	2,81	0,00	0,28
7	Pointed	0,00	0,00	0,04	0,17	0,02	7,89	2,39	0,41	6,13
8	Mountain side	0,00	0,00	0,00	0,05	0,00	12,32	0,86	0,00	0,20
	% sampling points	2,79	15,65	14,72	26,40	3,41	7,08	13,39	16,57	100

The last column of Table C1 shows that the IBGE map entails a class ("Convex") accounting alone for >60% of the area, which covers most of the territory apart from the coastal plains. These plains correspond to the second most extended class (14.3%). Logically, we note strong agreement between our landscape units relating to very flat/wet plains and IGBE classes relating to similar situations. We also note large agreement between our two units linked to Mountains and High tablelands and the "Pointed" (sharply convex) class of IBGE. The agreement also applied to IBGE classes of minor extent pertaining to strong reliefs. Our unit "Plains with residual relief" also match with several IBGE classes that are of limited extent but for "Tabular" (10.3%). The most extended IBGE class ("Convex") only showed weak associations with several of our landscape units pertaining to (High)-Tablelands, Hill and residual relief. It therefore appeared as heterogeneous. This suggests that an important advantage of our mapping is to propose distinctions within this very large class that is not very informative at the level of the State of Amapa.

3) Landscape map in French Guiana (Guitet et al., 2013)

Table C2
Cross-classification of 62,639 sampling points between classes of the landscapes map from Guitet et al. (2013) (rows) and the landscape units (present paper, columns). The last right-hand column and the bottom-row feature the percentages of sampling points in the different rows and columns, respectively. Relative frequencies above 1.5 are highlighted.

		Landscape types (present study)								
		Very wet plains	Very wet plains	Plains with residual reliefs	Hills	Residual reliefs	Tablelands	High Tablelands	Mountains	% Sampling points
Landscapes classes, Guitet et al. 2013		**8**	**1**	**4**	**6**	**7**	**2**	**5**	**3**	
Coastal plain	AC	26,52	16,24	2,48	0,00	0,33	0,01	0,14	0,11	3,03
Regular pattern hilly area	J	0,57	7,87	5,58	0,09	0,31	0,02	0,10	0,03	3,84
Plain with residual reliefs	AB	3,98	2,97	3,94	0,82	1,59	0,00	0,08	0,01	1,64
Inland plain	D	0,60	0,38	2,47	0,55	2,47	0,54	0,27	0,03	10,83
Low hilly area and large valley	C	0,00	0,50	1,12	3,06	0,72	0,37	0,31	0,06	4,89
Peneplain with moderate hill	I	0,26	0,29	0,91	2,98	1,13	0,23	0,25	0,16	8,49
Coastal plain with relief	AA	0,00	0,06	0,15	3,11	0,44	1,01	0,25	0,11	9,19
Moderate plateau	E	0,00	0,11	0,74	0,71	1,75	1,41	0,80	0,17	16,07
Hilly plateau with inselberg	F	0,00	0,07	0,25	0,51	0,59	2,35	1,18	0,35	6,82
High dissected plateau	G	0,00	0,02	0,22	0,16	0,32	2,83	1,25	0,30	7,47
Complex hilly area	B	0,32	0,35	0,75	0,93	1,03	0,96	1,77	0,84	11,25
High hill and mountain	H	0,00	0,07	0,12	0,01	0,48	0,15	2,57	4,99	16,48

From the cross-classification, we note the strong agreement between the two maps concerning the main coastal plains categories (i.e., AC vs. our classes 8 and 1) and hills (C vs. our 6). Logically, there is also excellent agreement for mountains (i.e., H versus our class 3), and good agreement regarding plateaus/tablelands (i.e., F and C vs. our class 2). In spite of these agreements, we also note that for each of our landscape units there is some scatter within several categories defined by Guitet et al. (2013). This reflects differences of methods and standpoints. There are twelve landscape categories in the typology of Guitet et al. (2013) compared to only eight in our present typology, which also addressed Amapa and, overall, aims to be more synthetic. The scattering into several categories is particularly important for our landscape unit "Plains with residual reliefs", that shows high relative frequencies with four landscape classes of Guitet et al. (2013). This unit mainly marks the fringe of the Guiana shield along the transition with the sedimentary coastal plain and therefore is liable to overlap with several classes. It also includes the "inland plain" class of Guitet et al. (2013), which is not distinguished in our present work because it is of limited extent and has a restricted distribution in the south of French Guiana.

References

Balaguer, A., Ruiz, L.A., Hermosilla, T., Recio, J.A., 2010. Definition of a comprehensive set of texture semivariogram features and their evaluation for object-oriented image classification. Comput. Geosci. 36 (2), 231–240.

Bispo, P.d.C, Dos Santos, J.R., Valeriano, M.d.M, Graça, P.M.L.d.A., Balzter, H., França, H., 2016. Predictive models of primary tropical forest structure from geomorphometric variables based on SRTM in the Tapajós region, Brazilian Amazon. PLoS One 11 (4). https://doi.org/10.1371/journal.pone.0152009.

Bizzi, L.A., Schobbenhaus, C., Gonçalves, J.H., Baars, F.J., Delgado, I.M., Abram, M.B., Neto, R.L., Matos, G.M.M., Santos, J.O.S., 2001. Geologia, Tectônica e Recursos Minerais do Brasil: Sistema de Informações Geográficas - SIG e Mapas na escala 1:2.500.000. CPRM, Brasília, Brazil.

Boaventura, F.M.C., Narita, C., 1974. Geomorfologia. Folha Na/NB.22-Macapá. Projeto Radam, Levantamento de Recursos Naturais, v.6. MME/DNPM, Rio de Janeiro, Brazil (pp. II/1-II/27).

Booth, A.M., Roering, J.J., Perron, J.T., 2009. Automated landslide mapping using spectral analysis and high-resolution topographic data: Puget sound lowlands, Washington, and Portland Hills, Oregon. Geomorphology 109, 132–147.

Bourgine, B., Baghdadi, N., 2005. Assessment of C-band SRTM DEM in a dense equatorial forest zone. C. R. Geosci. 337 (14), 1225–1234.

Choubert, B., 1957. Essai Sur la Morphologie de la Guyane. Imprimerie Nationale, Paris, France (109 pp).

Conrad, O., 2012. Module terrain Surface Convexity. The Comprehensive R Archive Network (CRAN).

Couteron, P., 2002. Quantifying change in patterned semi-arid vegetation by Fourier analysis of digitized aerial photographs. Int. J. Remote Sens. 23 (17), 3407–3425.

Couteron, P., Ollier, S., 2005. A generalized, variogram-based framework for multi-scale ordination. Ecology 86 (4), 828–834.

Couteron, P., Barbier, N., Gautier, D., 2006. Textural ordination based on Fourier spectral decomposition: a method to analyze and compare landscape patterns. Landsc. Ecol. 21 (4), 555–567.

Delor, C., Lahondère, D., Egal, E., Lafon, J.-M., Cocherie, A., Guerrot, C., Rossi, P., Truffert, C., Théveniaut, H., Phillips, D., Avelar, V.G., 2003. Transamazonian Crustal Growth and Reworking as Revealed by the 1:500 000 Scale Geological Map of French Guiana. 2nd edition. 2-3-4. Géologie de France, pp. 5–57.

Dragut, L., Eisank, C., 2012. Automated object-based classification of topography from SRTM data. Geomorphology 141–142, 21–33.

Dray, S., Jombart, T., 2011. Revisiting Gerry's data: introducing spatial constraints in multivariate analysis. Ann. Appl. Stat. 5 (4), 2278–2299.

Dray, S., Dufour, A.B., Thioulouse, J., 2016. Analysis of Ecological Data: Exploratory and Euclidean Methods in Environmental Sciences. The Comprehensive R Archive Network (CRAN) (409 pp).

Evans, I.S., 1972. General geomorphometry, derivatives of altitude, and descriptive statistics. In: Chorley, R.J. (Ed.), Spatial Analysis in Geomorphology. Methuen, London, UK, pp. 17–90.

Evans, I.S., 2012. Geomorphometry and landform mapping: what is a landform? Geomorphology 137, 94–106.

Farr, T.G., Rosen, P.A., Caro, E., Crippen, R., Duren, R., Hensley, S., Kobrick, M., Paller, M., Rodriguez, E., Roth, L., Seal, D., Shaffer, S., Shimada, J., Umland, J., Werner, M., Oskin, M., Burbank, D., Alsdorf, D., 2007. The shuttle radar topography mission. Rev. Geophys. 45 (2) (33 pp).

Fayad, I., Baghdadi, N., Bailly, J.S., Barbier, N., Gond, V., El Hajj, M., Fabre, F., Bourgine, B., 2014. Canopy height estimation in French Guiana with LiDAR ICESat/GLAS data using principal component analysis and random forest regressions. Remote Sens. 6, 11883–11914.

Figueiredo, F.O.G., Costa, F.R.C., Nelson, B.W., Pimentel, T.P., 2013. Validating forest types based on geological and land-form features in central Amazonia. J. Veg. Sci. 25 (1), 198–212.

Gibbs, A.K., Barron, C.N., 1993. The Geology of the Guiana Shield. Oxford Monographs on Geology and Geophysics 22, Oxford, UK (246 pp).

Guitet, S., Cornu, J.-F., Brunaux, O., Betbeder, J., Carozza, J.-M., Richard-Hansen, C., 2013. Landform and landscape mapping, French Guiana (South America). J. Maps 9 (3), 325–335.

Guitet, S., Pélissier, R., Brunaux Sabatier, D., Couteron, P., 2015a. Geomorphic control of rain-forest floristic composition in French Guiana: more than a soil filtering effect? J. Trop. Ecol. 32 (1), 22–40.

Guitet, S., Pélissier, R., Brunaux, O., Jaouen, G., Sabatier, D., 2015b. Geomorphological landscape features explain floristic patterns in French Guiana rainforest. Biodivers. Conserv. 24 (5), 1215–1237.

Guitet, S., Brunaux, O., de Granville, J.J., Gonzalez, S., Richard-Hansen, C., 2015c. Catalogue des habitats forestiers de Guyane. DEAL Guyane, Cayenne, French Guiana (120 pp).

Hammond, D.S., 2005. Tropical Forests of the Guiana Shield: Ancient Forests in a Modern World. CABI Publishing, Wallingford, UK (528 pp).

Hanley, J.T., 1977. Fourier analysis of the Catawba Mountain knolls, Roanoke County, Virginia. Math. Geol. 9 (2), 159–163.

Haralick, R.M., Shanmugam, K., Dinstein, I., 1973. Textural features for image classification. IEEE Trans. Syst. Man Cybern. 3, 610–621.

Harrison, J.M., Lo, C.P., 1996. PC-based two-dimensional discrete Fourier transform programs for terrain analysis. Comput. Geosci. 22 (4), 419–424.

Hijmans, R.J., 2016. Geographic Data Analysis and Modeling. The Comprehensive R Archive Network (CRAN) (244 pp).

Hua, B., Fu-long, M., Li-cheng, J., 2006. Research on computation of GLCM of image texture. Chin. J. Electron. 34 (1), 155–158.

Instituto Brasileiro de Geografia e estatistica (IBGE), 2004. Geomorfologia do Estado do Amapa, 1: 750,000. Base Cartográfica de Informações Ambientais por Estado, Ministério do Planejamento, Orçamento e Gestão, Diretoria de Geociências. (Electronic version available in:). ftp://geoftp.ibge.gov.br/informacoes_ambientais/geomorfologia/mapas/unidades_da_federacao/ap_geomorfologia.pdf.

Instituto Brasileiro de Geografia e estatistica (IBGE), 2015. Geomorfologia Amazônia Legal, 1: 250,000. Ministério do Planejamento, Orçamento e Gestão, Diretoria de Geociências. (Electronic version available in:). https://downloads.ibge.gov.br/downloads_geociencias.htm.

IRD, I.E.P.A., 2008. Programme de Cartographie des Littoraux Amazoniens. Série Ecossistemas costeiros, Carta Amapá Centro-Sul (AP-c), Scale 1:250,000. IEPA/IRD, Macapa, Brazil.

Iwahashi, J., Kamiya, I., 1995. Landform classification using digital elevation model by the skills of image processing—mainly using the Digital National Land Information. Geoinformatics 6 (2), 97–108 (in Japanese with English abstract).

Iwahashi, J., Pike, R.J., 2007. Automated classifications of topography from DEMs by an unsupervised nested-means algorithm and a three-part geometric signature. Geomorphology 86, 409–440.

Jaeger, J.A.G., Bertiller, R., Schwick, C., Müller, K., Steinmeier, C., Ewald, K.C., Ghazoul, J., 2008. Implementing landscape fragmentation as an indicator in the Swiss monitoring system of sustainable development (Monet). J. Environ. Manag. 88 (4), 737–751.

Jardim, K.A., Santos, V.F., Silveira, O.F.M., 2015. Uso de imagens SAR do sensor PALSAR/ALOS para mapeamento morfologico da regiao do Cabo Norte, Planicie Costeira do Amapa - Brasil. Contribuçoes à Geologia da Amazonia. 9, pp. 225–233.

Jordan, G., Schott, B., 2005. Application of wavelet analysis to the study of spatial pattern of morphotectonic lineaments in digital terrain models. Remote Sens. Environ. 94, 31–38.

Keitt, T.H., 2000. Spectral representation of neutral landscapes. Landsc. Ecol. 15, 479–493.

MacMillan, R.A., Shary, P.A., 2008. Chapter 9 landforms and landform elements in geomorphometry. Dev. Soil Sci. 33, 227–254.

MacMillan, R.A., MacNabb, D.H., Jones, R.K., 2000. Automated landform classification using DEMs a conceptual framework for a multi-level, hierarchy of hydrologically and geomorphologicaly oriented physiographic mapping units. 4th International Conference on Integrating GIS and Environmental Modeling (GIS/EM4): Problems, Prospects and Research Needs (Banff, Alberta, Canada. 16pp).

MacMillan, R.A., Martin, T.C., Earle, T.J., MacNabb, D.H., 2003. Automated analysis and classification of landforms using high-resolution digital elevation data: applications and issues. Can. J. Remote. Sens. 29, 592–606.

Magnani, A., 1952. As regiões naturais do Amapá. Rev. Bras. Geogr. 14 (3), 244–304.

Manly, B.J.F., 2004. Multivariate statistical methods. A Primer. Chapman and Hall/CRC Press, London, UK (224 pp).

Mark, D.M., 1975. Geomorphic parameters: a review and evaluation. Geographiska annaler: series A. Phys. Geogr. 57 (3/4), 165–177.

Migon, P., 2009. Are any granite landscapes distinctive of the humid tropics? Reconsidering multiconvex topographies. Singap. J. Trop. Geogr. 30, 327–342.

Mugglestone, M.A., Renshaw, E., 1998. Detection of geological lineations on aerial photographs using two-dimensional spectral analysis. Comput. Geosci. 24 (8), 771–784.

NASA JPL, 2013. NASA Shuttle Radar Topography Mission Global 1 Arc Second [Data set]. NASA EOSDIS Land Processes DAAC. https://doi.org/10.5067/MEaSUREs/SRTM/SRTMGL1.003.

Nir, D., 1957. The ratio of relative and absolute altitudes of Mt. Carmel: a contribution to the problem of relief analysis and relief classification. Geogr. Rev. 47 (4), 564–569.

Nobre, A.D., Cuartas, L.A., Hodnett, H., Renno, C.D., Rodrigues, G., Silveira, A., Waterloo, M., Saleska, S., 2011. Height above the nearest drainage – a hydrologically relevant new terrain model. J. Hydrol. 404, 13–29.

Ollier, S., Chessel, D., Couteron, P., Pélissier, R., Thioulouse, J., 2003. Comparing and classifying one-dimensional spatial patterns: an application to laser altimeter profiles. Remote Sens. Environ. 85, 453–462.

Paget, D., 1999. Etude de la Diversité Spatiale des Écosystèmes Forestiers Guianais: Réflexion Méthodologique et Application. PhD Thesis. Ecole Nationale du Génie Rural Des Eaux et Forêts, Nancy, France (155 pp.).

Panizza, M., 2009. The geomorphodiversity of the dolomites (Italy): a key of geoheritage assessment. Geoheritage 1 (1), 33–42.

Perron, J.T., Kirchner, J.W., Dietrich, W.E., 2008. Spectral signatures of characteristic spatial scales and nonfractal structure in landscapes. J. Geophys. Res. Earth Surf. 113:F04003. https://doi.org/10.1029/2007JF000866.

Pike, R.J., 1988. The geometric signature: quantifying landslide-terrain types from digital elevation models. Math. Geol. 20 (5), 491–511.

R Core Team, 2017. R: A Language and Environment for Statistical Computing. R Foundation for Statistical Computing, Vienna, Austria.

Renno, C.D., Nobre, A.D., Cuartas, L.A., Soares, J.V., Hodnett, M.G., Tomasella, J., Waterloo, M.J., 2008. HAND, a new terrain descriptor u sing SRTM-DEM: mapping terra-firme rainforest environments in Amazonia. Remote Sens. Environ. 112 (9), 3469–3481.

Sabatier, D., 2006. Evaluation Multi-Échelles de la Diversité Spécifique, Structurale et Fonctionnelle des Arbres en Forêt Guyanaise: Prise en Compte du Substrat Géologique, des Sols et de la Dynamique Sylvigénétique. Eosystèmes Tropicaux, Actes du 2ème Colloque de Restitution du Programme de Recherche. Ecofor - Ministère de L'écologie et du Développement Durable, Paris, France, pp. 125–133.

Sabatier, D., Grimaldi, M., Prevost, M.F., Guillaume, J., Godron, M., Dosso, M., Curmi, P., 1997. The influence of soil cover organization on the floristic and structural heterogeneity of a Guianan rain forest. Plant Ecol. 131 (1), 81–108.

Saerens, M., Fouss, F., Yen, L., Dupont, P., 2005. The principal components analysis of a graph and its relationships to spectral clustering. IAG Working Papers 124/04. Université Catholique de Louvain, Louvain, Belgium.

Santos, J.O.S., Hartmann, L.A., Gaudette, H.E., Groves, D.I., McNaughton, N.J., Fletcher, I.R., 2000. A new understanding of the provinces of the Amazon craton based on integration of field mapping and U-Pb and Sm-Nd geochronology. Gondwana Res. 3 (4), 453–488.

Silva, Uédio, Leite da, Robds, et al., 2006. Atlas da Zona Costeira Estuarina do Estado do Amapa: Do Diagnostico Socioambiental ao Zoneamento Ecologico-Economico Costeiro Participativo. Instituto de Pesquisas Científicas e Tecnológicas do estado do Amapa – IEPA, Macapa, Brazil (77 pp.).
Slaymaker, O., Spencer, T., Embleton-Haman, C., 2009. Geomorphology and Global Environment Change. Cambridge University Press, Cambridge, UK (468 pp).
Stoica, P., Moses, R., 2005. Spectral Analysis of Signals. Prentice Hall, Upper Saddle River, NJ.
Thomas, M.F., 2006. Lessons from the tropics for a global geomorphology. Singap. J. Trop. Geogr. 27 (2), 111–127.
Trevisani, S., Cavalli, M., Marchi, L., 2012. Surface texture analysis of a high-resolution DTM: interpreting an alpine basin. Geomorphology 161-162, 26–39.
Vogt, P., Riitters, K.H., Estreguil, C., Kozak, J., Wade, T.G., Wickham, J.D., 2007. Mapping spatial patterns with morphological image processing. Landsc. Ecol. 22, 171–177.
Walsh, R.P.D., Blake, W.H., Slaymaker, O., Spencer, T., 2009. Tropical rainforests. In: Embleton-Haman, C. (Ed.), Geomorphology and Global Environmental Change. Cambridge University Press, Cambridge, UK, pp. 214–243.